

1 **Enrichment of calcium in sea spray aerosol: ~~through~~ Insights from bulk**
2 **measurements and individual particle analysis during the R/V *Xuelong* cruise**
3 **in ~~over~~ the summertime Ross Sea, Antarctica**

4 Bojiang Su ^{a,b}, Xinhui Bi ^{a,c}, Zhou Zhang ^{b,d}, Yue Liang ^e, Congbo Song ^f, Tao Wang ^{a,b}, Yaohao
5 Hu ^{a,b}, Lei Li ^{g,*}, Zhen Zhou ^g, Jinpei Yan ^h, Xinming Wang ^{a,c}, Guohua Zhang ^{a,c,*}

6 ^a State Key Laboratory of Organic Geochemistry and Guangdong Provincial Key Laboratory of
7 Environmental Protection and Resources Utilization, Guangzhou Institute of Geochemistry,
8 Chinese Academy of Sciences, Guangzhou 510640, China

9 ^b University of Chinese Academy of Sciences, Beijing 100049, China

10 ^c Guangdong-Hong Kong-Macao Joint Laboratory for Environmental Pollution and Control,
11 Guangzhou 510640, China

12 ^d State Key Laboratory of Isotope Geochemistry, Guangzhou Institute of Geochemistry, Chinese
13 Academy of Sciences, Guangzhou 510640, China

14 ^e Department of Civil and Environmental Engineering, Faculty of Science and Technology,
15 University of Macau, Taipa, Macau, China

16 ^f National Centre for Atmospheric Science (NCAS), University of Manchester, Manchester M13
17 9PL, UK

18 ^g Institute of Mass Spectrometry and Atmospheric Environment, Jinan University, Guangzhou
19 510632, China

20 ^h Key Laboratory of Global Change and Marine-Atmospheric Chemistry, Third Institute of
21 Oceanography, Ministry of Natural Resources, Xiamen 361005, China

22 *Corresponding author: zhanggh@gig.ac.cn; lileishdx@163.com

23 **Abstract:** ~~€Although~~ calcium is known to be enriched in sea spray aerosols (SSAs), ~~but its~~
24 ~~controlling~~the factors ~~and individual mixing states~~that affect its enrichment remain ambiguous.
25 ~~Here, we investigate the impact of various~~~~In this study, we examine how~~ environmental factors
26 ~~affect the~~ ~~on the~~distribution of water-soluble calcium (Ca²⁺) distribution in SSAs. ~~We obtained our~~
27 ~~dataset from observations taken during a research cruise on the~~ ~~through~~ R/V *Xuelong* cruise ~~in~~
28 ~~observations~~over the Ross Sea, Antarctica, from December 2017 to February 2018. ~~We~~
29 ~~observed~~Our observations showed that the ~~enhanced~~ Ca²⁺-enrichment ~~of Ca²⁺~~ in aerosol samples
30 ~~was enhanced under specific conditions, including~~ ~~at~~ lower temperatures (< -3.5 °C), lower wind
31 speeds (< 7 m s⁻¹), and ~~in~~ the presence of sea ice. ~~Our analysis of~~ ~~Further~~ individual particle mass
32 spectral~~analysis indicated~~ ~~revealed~~ that ~~a significant~~ ~~considerable~~ ~~fractions~~ ~~portion~~ of calcium in
33 SSAs likely ~~bound~~ ~~bind~~ with organic matter (~~in the form of a~~ single-particle type, OC-Ca), ~~Our~~
34 ~~findings suggest that current estimations of~~ ~~which may be neglected in current water-soluble~~
35 ~~estimation of~~ Ca²⁺ enrichment ~~based solely on water-soluble Ca²⁺~~ may be inaccurate. Also,
36 ~~this~~Our study is the first ~~to observe time that~~ a calcium-dominated single-particle type ~~dominated~~
37 ~~by calcium~~ ~~has been observed~~ in the Antarctic atmosphere. ~~We~~ ~~Our findings~~ suggest that ~~a broader~~
38 ~~focus on individual OC-Ca and its subsequent environmental behavior should be included in~~
39 future Antarctic atmospheric modeling ~~should take into account the environmental behavior of~~
40 ~~individual OC-Ca.~~ ~~Given the context of~~ ~~With the ongoing~~ global warming and ~~sea ice~~ ~~retreat of sea~~
41 ~~ice,~~ ~~it is essential to~~ ~~an~~ understanding ~~of~~ the mechanisms of calcium enrichment and ~~the~~ mixing
42 state of individual particles ~~to better comprehend~~ ~~involved is valuable for further recognizing the~~
43 ~~aerosol-cloud-climate~~ ~~the~~ interactions ~~between aerosols, clouds, and climate~~ ~~during~~ ~~in~~ the
44 Antarctica summer.

45 **Key points:**

46 ● ~~Enhanced~~ Ca^{2+} enrichment in sea spray aerosols (SSAs) was observed at lower ambient
47 temperatures, lower wind speeds, and in the presence of sea ice.

48 ● Individual particle analysis revealed a ~~large proportions~~ significant portion of internally mixed
49 organics with calcium particles in the Antarctic summer atmosphere.

50 ● ~~Organically complexed calcium may be neglected in current water-soluble estimation of Ca^{2+}~~
51 ~~enrichment in SSA.~~

52 ● Current water-soluble estimation of Ca^{2+} enrichment in SSAs may be inaccurate without
53 considering organically complexed calcium.

54 **Key-words:** Sea spray aerosol; Calcium enrichment; Individual particle analysis; Environmental
55 factors; Internally mixed organics with calcium particles; Antarctic summer atmosphere.

56

57 **1 Introduction**

58 Sea spray aerosols (SSAs) govern radiative forcing by directly scattering and absorbing solar
59 radiation over the remote ocean (Murphy et al., 1998), and they affect the microphysical properties
60 of marine clouds by serving as cloud condensation nuclei (CCN) and ice nuclei (IN) (Wilson et al.,
61 2015; Brooks and Thornton, 2018; Willis et al., 2018). Calcium is one of the components of
62 ~~SSASSAs~~, which can present as inorganic calcium (e.g., CaCl₂ and CaSO₄) (Chi et al., 2015) as
63 well as organic calcium (i.e., Ca²⁺ can readily induce the gelation of organic matter, presenting as
64 the most efficient gelling agent) (Carter-Fenk et al., 2021). ~~The extent of Calcium~~ enrichment and
65 chemical signature ~~of calcium may can~~ affect some physicochemical properties of ~~SSASSA~~ such
66 as alkalinity and hygroscopicity (Salter et al., 2016; Mukherjee et al., 2020), which is critical for
67 understanding aerosol-cloud interactions over the remote marine boundary layer (Keene et al.,
68 2007; Leck and Svensson, 2015; Bertram et al., 2018).

69 ~~A growing number of~~ Several studies have ~~shown that~~ demonstrated significant enrichment of
70 calcium (Ca²⁺) ~~is significantly enriched in SSASSAs relative compared to bulk seawater, as~~
71 briefly summarized in (Table S1) and documented by Keene et al. (2007), Hara et al. (2012),
72 Cochran et al. (2016), Salter et al. (2016), Cravigan et al. (2020), and Mukherjee et al. (2020). For
73 example, Hara et al. (2012) found that the Ca²⁺ enrichment of aerosol samples was sensitive to sea
74 salt fractionation during the cold winter-spring season over the Antarctic coast. Leck and Svensson
75 (2015) suggested that Ca²⁺ enrichment in SSAs is attributed to bubble bursts on sea ice leads
76 ~~within the sea ice~~ over the Arctic area. Similarly, low wind-driven bubble bursts were regarded as

77 a major reason for the Ca^{2+} enrichment in SSAs during an Arctic cruise (Mukherjee et al., 2020).
78 These results ~~have greatly improved the understanding of the processes contributing to shed light~~
79 ~~on the~~ Ca^{2+} enrichment process; however, our understanding of how environmental factors
80 synergistically affect such enrichment processes remains unclear.

81 To date, a unified consensus on the chemical form of calcium to explain calcium enrichment
82 in SSAs has not been reached. The enrichment extent of calcium and its chemical form in SSA
83 ~~have been deduced with water-soluble Ca^{2+} .~~ Two hypotheses have been proposed: (i) Calcium
84 enrichment is dominated by inorganic calcium, such as CaCO_3 and CaCl_2 . Ca^{2+} is enriched close
85 to the seawater surface in the form of ionic clusters (most probably with carbonate ions) (Salter et
86 al., 2016). Another source of CaCO_3 is directly from calcareous shell debris (Keene et al., 2007).
87 Through bubble bursts, both CaCO_3 and CaCl_2 along with sea salt can be emitted into the
88 atmosphere. In addition, the sea salt fractionation by precipitation of ikaite ($\text{CaCO}_3 \cdot 6\text{H}_2\text{O}$) may
89 contribute to calcium enrichment in aerosol during the freezing of sea ice (Hara et al.,
90 2012). ~~(Dieckmann et al., 2008; Dieckmann et al., 2010; Hara et al., 2012)~~ calcium enrichment is
91 dominated by inorganic calcium, such as CaCl_2 and $\text{CaCO}_3 \cdot 6\text{H}_2\text{O}$ (ikaite), derived from wind-
92 blown bubble bursts, calcareous shell debris and/or sea salt fractionation (Keene et al., 2007;
93 ~~Dieckmann et al., 2008; Hara et al., 2012).~~ (ii) Calcium enrichment is attributed to organically
94 complexed calcium. Ca^{2+} may bind with organic matter, which is relevant with marine microgels
95 and/or coccolithophore phytoplankton scales, and can be emitted by bubble bursting (Oppo et al.,
96 1999; Sievering, 2004; Leck and Svensson, 2015; Cochran et al., 2016; Kirpes et al., 2019;
97 Mukherjee et al., 2020). The chemical form of calcium can ~~significantly~~ determine its atmospheric
98 role, ~~and~~ inorganic calcium may exhibit stronger aerosol alkalinity and hygroscopicity than

99 organic calcium (Salter et al., 2016; Mukherjee et al., 2020). However, current estimations of
100 calcium enrichment based solely on water-soluble Ca²⁺ may not precisely explain the calcium
101 distribution in SSAs. This is because the amount of low water-soluble complexation of Ca²⁺ with
102 organic matter (e.g., aged Ca²⁺-assembled gel-like particles) (Orellana and Verdugo, 2003; Leck
103 and Bigg, 2010; Russell et al., 2010; Orellana et al., 2011; Leck and Svensson, 2015) and
104 insoluble Ca²⁺ in the form of calcareous shell debris or the like may not be considered, because
105 organic calcium has low water solubility (e.g., aged Ca²⁺-assembled gel-like particles) (Orellana
106 and Verdugo, 2003; Leck and Bigg, 2010; Russell et al., 2010; Orellana et al., 2011; Leck and
107 Svensson, 2015), the commonly measured water-soluble Ca²⁺ may not precisely explain the
108 calcium distribution in SSA. Thus, an understanding Thus, an alternative method, such as
109 discerning the mixing state based on single-particle analysis, of the mixing state of individual
110 calcareous aerosols may provide unique insights into the chemical form of calcium, and thus the
111 mechanisms of calcium enrichment in SSAs.

112 As a part of the 34th Chinese Antarctic Research Expedition (CHINARE ANT34th), ~~the aim~~
113 ~~of this~~ study aimed was to investigate the influencing factors and possible mechanisms of calcium
114 enrichment in SSASSAs through R/V *Xuelong* cruise observation campaigns over the Ross Sea,
115 Antarctica. An in-situ gas and aerosol composition monitoring system (IGAC) was employed to
116 determine the extent of Ca²⁺ enrichment in SSASSAs. Single-particle aerosol mass spectrometry
117 (SPAMS) was utilized to measure the size and chemical signature (i.e., mixing state) of individual
118 calcareous particles. We first investigated the impact of environmental factors such as ambient
119 temperature, wind speed, sea ice fraction, ~~and~~ chlorophyll-a concentration, and back trajectory

120 coverage on Ca²⁺ enrichment in SSASSAs. Then, the mechanisms of calcium enrichment in
121 SSASSAs were inferred according to the mixing state of individual calcareous particles.

122 **2 Methodology**

123 **2.1 The R/V *Xuelong* cruise and observation regions**

124 Our study focused on the Ross Sea region of Antarctica (50 to 78° S, 160 to 185° E) (Fig. 1),
125 where we conducted two separate observation campaigns aboard the R/V *Xuelong*. During
126 sampling the observations, this region was relatively isolated from the impact of long-range
127 transport of anthropogenic aerosols and has experienced the sea ice retreat (Yan et al., 2020a).

128 The first observation campaign (Leg I) took place from December 2-20, 2017, during the sea
129 ice period. The second campaign (Leg II) was conducted from January 13 to February 14, 2018,
130 during the period without sea ice. The sampling design for Leg I and Leg II aimed to investigate
131 how changing environmental factors affect the enrichment extent of calcium and the
132 characteristics of individual particles.

133 ~~Two observations were carried out aboard the R/V *Xuelong* cruise over the Ross Sea,~~
134 ~~Antarctica (50 to 78° S, 160 to 185° E) (Fig. S1). During sampling, this region was relatively~~
135 ~~isolated from the impact of long range transport of anthropogenic aerosols and has experienced~~
136 ~~the sea ice retreat (Yan et al., 2020a). The first leg of the cruise (leg I) was conducted from 2-20~~
137 ~~December, 2017, when the ocean was covered by sea ice. The second leg of the cruise (leg II) was~~
138 ~~carried out in the same region from January 13 to February 14, 2018, when basically no sea ice~~
139 ~~presents. Therefore, legs I and II were also regarded as the “sea ice period” and “the period~~
140 ~~without sea ice”, respectively, hereafter.~~

141 **2.2 ~~Metrological~~ Meteorological parameters and satellite data of air masses, sea ice, and**
142 **chlorophyll-a**

143 ~~We measured various m~~Meteorological parameters, ~~including such as~~ ambient temperature,
144 relative humidity (RH), wind speed, and true wind direction ~~were measured by using~~ an automated
145 meteorological station ~~located~~ on the top deck of the R/V *Xuelong* (**Fig. S2-S1 and Table S2**).

146 ~~To determine the type of air masses, we first overviewed the 72-hour back trajectory with~~
147 ~~daily resolution per each starting location by using the NOAA Hybrid Single-Particle Lagrangian~~
148 ~~Integrated Trajectories (HYSPLIT, version 4.9) model (Fig. S2). Additionally, we conducted a 96-~~
149 ~~hour back trajectory analysis with an hourly resolution, which covered the enhanced calcium~~
150 ~~enrichment events associated with sea ice fraction and chlorophyll-a concentration (discussed in~~
151 ~~section 3.1), using the TrajStat in Meteoinfo (version 3.5.8) (Wang et al., 2009; Wang, 2014).~~
152 ~~Meteorological data used for back trajectory analysis obtained from the Global Data Assimilation~~
153 ~~System (GDAS, ftp://ftp.arl.noaa.gov/pub/archives). Moreover, The type of air masses was~~
154 ~~calculated by 72-hour back trajectory analysis using the NOAA Hybrid Single-Particle Lagrangian~~
155 ~~Integrated Trajectories (HYSPLIT, version 4.9) model (Fig. S1). we obtained t~~The monthly sea
156 ice fraction ~~was obtained~~ from the Sea Ice Concentration Climate Data Record with a spatial
157 resolution of 25 km ([https://www.ncei.noaa.gov/products/climate-data-records/sea-ice-](https://www.ncei.noaa.gov/products/climate-data-records/sea-ice-concentration)
158 [concentration](https://www.ncei.noaa.gov/products/climate-data-records/sea-ice-concentration)) ~~and, t~~The 8-day chlorophyll-a concentration ~~was collected~~ from MODIS-aqua with
159 a spatial resolution of 4 km (<https://modis.gsfc.nasa.gov>) (**Fig. S3**).

160 During the R/V *Xuelong* cruise observation ~~campaigns~~, leg I was dominantly affected by the
161 ~~72-h~~ air masses from the sea ice-covered open-~~water~~ (~~7892%~~, ~~by trajectory coverage~~), and leg II
162 was mainly affected by the ~~72-h~~ air masses from continental Antarctica (~~4058%~~) (**Fig. S1 and**

163 **Table S1+S2**). The average ambient temperature (-4.0 ± 1.4 °C vs. -3.1 ± 2.2 °C), wind speed ($7.2 \pm$
164 5.5 m s⁻¹ vs. 7.1 ± 4.2 m s⁻¹), and chlorophyll-a concentration (0.51 ± 0.29 µg L⁻¹ vs. 0.44 ± 0.18
165 µg L⁻¹) varied slightly between legs I and II (**Table S2**).

166 **2.3 Contamination control during observation campaigns**

167 During the research cruise, the major contamination source was identified as emissions from
168 a chimney located at the stern of the vessel and about 25 m above the sea surface. To mitigate the
169 potential impact of ship emissions on aerosol sampling, we have taken several measures. Firstly, a
170 total suspended particulate (TSP) sampling inlet connecting to the monitoring instruments was
171 fixed to a mast 20 m above the sea surface, located at the bow of the vessel. In addition, the
172 sampling inlet was fixed on a ship pillar with a rain cover, which could minimize the potential
173 influence of violent shaking of the ship and sea waves. Secondly, sampling was only conducted
174 while the ship was sailing, to avoid the possible effect of ship emission on aerosol sampling under
175 the low diffusion condition. Lastly, we did not observe the mass spectral characteristics associated
176 with ship emission (e.g., particles simultaneously contain m/z 51 [V]⁺, 67 [VO]⁺, and element
177 carbon) during the observation campaigns (Liu et al., 2017; Passig et al., 2021). These measures
178 ensured that the collected data were representative and reliable for subsequent analysis.92

179 **2.4.3 Instrumentation**

180 An IGAC (Model S-611, Machine Shop, Fortelice International Co. Ltd., Taiwan, China) and
181 a SPAMS (Hexin Analytical Instrument Co., Ltd., China) were synchronously employed to
182 determine water-soluble ion mass concentrations of bulk aerosol and the size and chemical
183 composition of individual particles in real-time with hourly resolution (Figs. 2 and S4). In the

184 aerosol sampling procedure, a TSP inlet with a PM₁₀ cyclone (trap efficiency greater than 99% for
185 particles > 0.3 μm, D_{a50} = 10 ± 0.5 μm) was used for IGAC sampling and a PM_{2.5} cyclone (D_{a50} =
186 2.5 ± 0.2 μm) to remove particles larger than 2.5 μm for SPAMS. All instruments were connected
187 using conductive silicon tubing with an inner diameter of 1.0 cm.

188 **2.34.1 Aerosol water-soluble ion constituents**

189 ~~(Model S-611, Machine Shop, Fortelice International Co. Ltd., Taiwan, China)~~ An IGAC
190 ~~(Model S-611, Machine Shop, Fortelice International Co. Ltd., Taiwan, China)~~ was applied to
191 determine the water-soluble ion mass concentrations of aerosol (Fig. S4). Notably, only the water-
192 soluble fraction (organic and inorganic) of the aerosols sampled was considered (details in
193 Supporting Information, SI text S1) (Oppo et al., 1999). Sampling was performed only while the
194 ship was sailing. A PM₁₀ cyclone with trap efficiency larger than 99% was fixed to a bow mast at
195 20 m above the sea surface for IGAC sampling to minimize the impact of stern emissions. The
196 details of the analytical method ~~and ion mass concentrations of~~ IGAC have been described in
197 previous studies (Young et al., 2016; Yan et al., 2019; Yan et al., 2020b). Briefly, the IGAC system
198 consisted of three main units, including a Wet Annular Denuder (WAD), a Scrub and Impact
199 Aerosol Collector (SIAC), and an ion chromatograph (IC, Dionex ICS-3000) (Fig. 2). Gases and
200 aerosols were passed through WAD with a sampling flow of 16.7 L min⁻¹. Two concentric Pyrex
201 glass cylinders with a length of 50 cm and inner and outer diameters of 1.8 and 2.44 cm were
202 assembled to WAD, in which the inner walls of the annulus were wetted with ultrapure water (18.2
203 MΩ cm⁻¹). This part was responsible for the collection of acidic and basic gases by diffusion and
204 absorption of a downward-flowing aqueous solution. The SIAC had a length of 23 cm and a

205 diameter of 4.75 cm, which was positioned at an angle to facilitate the collection of enlarged
206 particles. The collected particles were separated firstly, continually enlarged by vapor steam, and
207 then accelerated through a conical-shaped impaction nozzle and collected on an impaction plate.
208 Each aerosol sample was collected for 55 minutes and injected for 5 minutes. The injection loop
209 size was 500 μL for both anions and cations, which were subsequently analyzed by IC. The
210 collection efficiency of aerosol and gas samples before they entered IC was previously reported
211 higher than 89% (for 0.056 μm particles, 89%; for 1 μm particles, 98%; for gaseous samples, >
212 90%) (Chang et al., 2007; Tian et al., 2017). The target ion concentrations were calibrated with a
213 coefficient of determination (r^2) above 0.99 by using standard solutions (0.1-2000 $\mu\text{g L}^{-1}$). The
214 detection limits for Na, Cl, Ca, K, and Mg were 0.03, 0.03, 0.019, 0.011, and 0.042 $\mu\text{g L}^{-1}$
215 (aqueous solution), respectively. The systematic error of the IC systems was generally less than
216 5%. The detection limits for Na^+ , Cl^- , Ca^{2+} , K^+ , and Mg^{2+} were 0.03, 0.03, 0.019, 0.011, and 0.042
217 $\mu\text{g L}^{-1}$ (aqueous solution), respectively. ~~During~~
218 ~~Throughout the whole observation~~ the observation scampaigns, the mean Na^+ and Ca^{2+} mass
219 concentrations were 364.64 ng m^{-3} (ranging from 6.66 to 4580.10 ng m^{-3}) and 21.20 ng m^{-3}
220 (ranging from 0.27 to 334.40 ng m^{-3}), respectively, which were ~~far above (>10 times)~~ higher than
221 the detection limits. ~~In comparison with the whole measurement (21.2 ng m^{-3}), the mean Ca^{2+}~~
222 ~~mass concentrations were lower at low wind speeds (17.3 ng m^{-3} at $< 7 \text{ m s}^{-1}$ and 15.0 ng m^{-3} at $<$~~
223 ~~3 m s^{-1}).~~ ~~Therefore, the impact of ship emissions on the Ca^{2+} mass concentration could be~~
224 ~~negligible under the low wind conditions.~~ Analytical uncertainty of Ca^{2+} enrichment based on
225 water-soluble analysis was estimated at less than 11% (Supporting Information, SI text S3S1).
226 It should be clarified that the water-soluble ion mass concentration included the pure

227 inorganic part (e.g., pure sea salt, NaCl) and mixed organic-inorganic part (e.g., gel-like particles)
228 (Quinn et al., 2015). Numerous studies have reported that primary SSA exhibited moderate
229 hygroscopicity and water solubility due to a certain water-soluble organic fraction (~ 25%, by
230 mass), such as carboxylates, lipopolysaccharides (LPSs), humic substances, and galactose (Oppo
231 et al., 1999; Quinn et al., 2015; Schill et al., 2015; Cochran et al., 2017). For example, Oppo et al.
232 (1999) indicated that humic substances were an important pool of water-soluble natural surfactants
233 (40-60%) in marine surfactant organic matter. In addition, LPSs are preferentially transferred to
234 submicron SSA during bubble bursting and exhibit a certain solubility of 5 g L⁻¹ in pure water.
235 (Facchini et al., 2008; Schill et al., 2015). Therefore, both organic and inorganic parts with a
236 water-soluble nature could be retained, contributing to the water-soluble ion mass concentration
237 (e.g., Ca²⁺).

238 **2.34.2 Single-particle analysis**

239 ~~The size and chemical signature of individual particles were obtained in real time by a~~
240 ~~SPAMS (Hexin Analytical Instrument Co., Ltd., China) (Fig. S4).~~ A brief description of ~~the~~
241 SPAMS ~~has been~~ provided elsewhere (Li et al., 2011). Briefly, the aerosols were drawn into
242 SPAMS by a PM_{2.5} inlet after a silica gel dryer (**Fig. 2**). A collimated particle beam focused by an
243 aerodynamic lens ~~was~~ then accelerated in an accelerating electric field and passed through two
244 continuous laser beams (Nd: YAG laser, 532 nm). The obtained time of flight (TOF) and velocity
245 of individual particles were used to calculate the vacuum aerodynamic diameter (D_{va}) based on a
246 calibration curve. Subsequently, particles with a specific velocity were desorbed and ionized by
247 triggering a pulse laser (an Nd: YAG laser, 266 nm, 0.6 ± 0.06 mJ was used in this study). The ion

248 fragments were recorded using a bio-polar TOF mass spectrometer. ~~Prior to~~Before the use of
249 SPAMS, standard polystyrene latex spheres (0.2-2 μm , Duke Scientific Corp., Palo Alto, CA) and
250 PbCl_2 and NaNO_3 (0.35 μm , Sigma-Aldrich) solutions were used for the size and mass spectral
251 calibration, respectively. The hit rate, defined as the ratio of ionized particles to all sampled
252 particles, of the SPAMS ~~is~~was $\sim 11\%$ during the cruise observation campaigns.

253 During the R/V *Xuelong* cruise observation campaigns, approximately 930,000 particles with
254 mass spectral fingerprints and D_{va} ranging from 0.2 to 2 μm were measured. An adaptive
255 resonance theory neural network (ART-2a) was used to group~~ed~~ the particles into several clusters
256 based on their mass spectral fingerprints, using parameters of a vigilance factor of 0.85, a learning
257 rate of 0.05, and a maximum of 20 iterations (Song and Hopke, 1999). The manually obtained
258 clusters were sea salt (SS, 16.5%), aged sea salt (SS-aged, 8.1%), sea salt with biogenic organic
259 matter (SS-Bio, 3.1%), internally mixed organics with calcium (OC-Ca, 48.7%), internally mixed
260 organics with potassium (OC-K, 13.7%), organic-carbon-dominated (OC, 7.0%), and element
261 carbon (EC, 2.9%) (**Fig. S5 and Table S3**) (Prather et al., 2013; Collins et al., 2014; Su et al.,
262 2021). All single-particle types had marine origins with typical mass spectral characteristics of Na
263 (m/z 23), Mg (m/z 24), K (m/z 39), Ca (m/z 40), and Cl (m/z -35 and -37), except for EC (**SI text**
264 **S4S2**). There was little difference in individual particle analysis regarding chemical composition,
265 size, and mixing state of particle clusters obtained from leg I and leg II (SI Text S3).

266 **3 Results**

267 **3.1 Ca^{2+} enrichment dominated by environmental factors**

268 We propose that both Na^+ and Ca^{2+} in our observations originated from marine sources.

269 The mass concentration of Na⁺ exhibited a strong positive correlation with that of Cl⁻ (r = 0.99,
270 p < 0.001) and Mg²⁺ (r = 0.99, p < 0.001) (Fig. S6), indicating that they had a common origin
271 (i.e., sea spray). However, it is not surprising that the mass concentration of Na⁺ showed a
272 relatively weak correlation with that of Ca²⁺ (r = 0.51, p < 0.001) (Fig. S6). This can be
273 explained by the low water-soluble complexation of Ca²⁺ with organic matter and/or insoluble
274 Ca²⁺ in the form of calcareous shell debris, such as CaCO₃. In addition, the potential impact of
275 long-range transport of anthropogenic aerosols and dust contributing to Ca²⁺ may be limited due
276 to the predominance of polar air masses during the observation campaigns (Fig. S2).

277 The enrichment factor (EF_x), defined as the mass concentration ratio of a specific species
278 X to Na⁺ in aerosols to that in bulk seawater, is generally used to describe the enrichment extent
279 of species X in aerosols.

$$280 \quad EF_x = \frac{([X]/[Na^+])_{aerosol}}{([X]/[Na^+])_{seawater}}$$

281 An EF_x > 1 indicates a positive enrichment; otherwise, it indicates depletion. ~~The~~
282 ~~measurements were almost entirely influenced by polar air masses (Fig. S1). Therefore, the long-~~
283 ~~range transport of anthropogenic aerosols may be limited. All Na⁺ was assumed to originate from~~
284 ~~SSA.~~ Generally, the ratio of Ca²⁺ to Na⁺ in seawater is 0.038 (w/w) (Boreddy and Kawamura,
285 2015; Su et al., 2022). During the whole cruise, the hourly average EF_{Ca} was 2.76 ± 6.27 (mean ±
286 standard deviation (M ± SD), n = 1051, ranged from 0.01 to 85, median = 1.18, interquartile range
287 (IQR) = 1.85). Similar to previous studies (Salter et al., 2016), positive magnesium (Mg²⁺) and
288 potassium (K⁺) enrichment in ~~SSASSAs~~ was also observed (SI text ~~S5S4~~).

289 ~~Figure 1-3 shows presents~~ the enrichment factor of Ca²⁺ (EF_{Ca}) at different ambient
290 temperatures (separated by a mean value of -3.5 °C), wind speeds (separated by a mean value of 7

291 m s⁻¹), and ~~with/without~~ in the presence/absence of sea ice during ~~the whole cruise~~ the entire
292 observation campaign. The results ~~clearly~~ indicated that the highest EF_{Ca} zone (M ± SD = 3.83 ±
293 3.43, median = 2.66, IQR = 3.37, n = 144) ~~appeared-occurred~~ at a relatively a lower ambient
294 temperature (< -3.5 °C), lower wind speed (< 7 m s⁻¹) and in the presence of sea ice (**Fig. 3dS6**).
295 Compared to the contrary conditions (i.e., ambient temperatures ≥ -3.5 °C, wind speeds ≥ 7 m s⁻¹,
296 and the absence of no sea ice), there was almost calcium depletion (EF_{Ca}, M ± SD = 1.01 ± 0.80,
297 median = 0.70, IQR = 0.73, n = 182) (Fig. 3c). Notably, we observed a higher EF_{Ca} during the sea
298 ice period than during the period without sea ice (3.83 ± 3.43 vs. 2.45 ± 3.09 by M ± SD and 2.66
299 vs. 1.18, by median) (Fig. 3d), under the conditions of ambient temperatures < -3.5 °C and wind
300 speeds < 7 m s⁻¹. In addition, we also observed more frequent Ca²⁺ enrichment events during the
301 sea ice period (71.0% in leg I) compared to the period without sea ice (47.7% in leg II) (Table S2).
302 Moreover, the increased EF_{Ca} varied with decreasing ambient temperature and wind speed and
303 with increasing sea ice fraction, as shown in Fig. 4. Taken together, our results indicate that the
304 enhanced Ca²⁺ enrichment in SSAs is sensitive to the lower temperature, lower wind speeds, and
305 the presence of sea ice.

306 Under the conditions of ambient temperatures < -3.5 °C and wind speeds < 7 m s⁻¹, a higher
307 EF_{Ca} was observed during the sea ice period than during the period without sea ice (3.83 ± 3.43 vs.
308 2.45 ± 3.09 by M ± SD and 2.66 vs. 1.18, by median) (Fig. S6). ~~The EF_{Ca} increased with~~
309 ~~decreasing ambient temperature and wind speed, as also shown in Fig. 2~~. In addition, the positive
310 ~~Ca²⁺ enrichment events (71%) were most associated with leg I, that is, air masses blowing from~~
311 ~~the large fraction of sea ice covered ocean (i.e., Ross Sea, 78%) (Table S1)~~. And there was a
312 ~~positive correlation (r = 0.73, p < 0.01) between the sea ice fraction and EF_{Ca} during leg I (sea ice~~

313 period) (Fig. 2), indicating a possible effect of the presence of sea ice on Ca^{2+} enrichment in SSA.
314 ~~Under the conditions of ambient temperatures ≤ 3.5 °C and wind speeds ≤ 7 m s⁻¹, a higher EF_{Ca}~~
315 ~~was observed during the sea ice period than during the period without sea ice (3.83 ± 3.43 vs. 2.45~~
316 ~~± 3.09 by $M \pm \text{SD}$ and 2.66 vs. 1.18 , by median) (Fig. S6). In contrast, under the conditions of~~
317 ~~ambient temperatures ≥ 3.5 °C, wind speeds ≥ 7 m s⁻¹, and no sea ice, there was almost calcium~~
318 ~~depletion (EF_{Ca} , $M \pm \text{SD} = 1.01 \pm 0.80$, median = 0.70 , IQR = 0.73 , $n = 182$) in the SSA (Fig. S6).~~

319 We further analyzed the distribution of Ca^{2+} enrichment concerning 96-hour back trajectories
320 with sea ice fraction and chlorophyll-a concentration, as shown in Fig. 5. During the observation
321 campaigns, we identified five areas with the continuous enhancement of Ca^{2+} enrichment, namely,
322 Area 1 and 2 during the leg II, and Area 3,4, and 5 during the leg I. Our results indicated that air
323 masses traveling over the sea ice and marginal ice zone ($> 95\%$, by trajectory coverage) in Areas 3,
324 4, and 5, as well as those over the sea ice (28%-33%) and land-based Antarctic ice (57-59%) in
325 Area 1 and 2, were strongly associated with the increased calcium enrichment (Table S4). These
326 pieces of evidence further support the influence of sea ice on the increased calcium enrichment,
327 while simultaneously ruling out the influence of long-range transport of anthropogenic aerosol and
328 dust outside the Antarctic.

329 ~~We~~ We observed ~~noted~~ that a series of high EF_{Ca} cases in ~~(Area 1)~~ were correlated with
330 associated with a high concentration of chlorophyll-a ($0.99 \pm 1.65 \mu\text{g L}^{-1}$) during leg II (Fig. S7
331 and Table S4). However, it is unlikely that ~~the~~ phytoplankton and/or bacteria are responsible for
332 the enhanced EF_{Ca} cases ~~was unlikely to be attributed to phytoplankton and/or bacteria~~ due to the
333 ~~poor~~ weak correlation ($r = 0.12$, $p < 0.01$) between the chlorophyll-a concentration and EF_{Ca}
334 values (Fig. ~~S8~~ S7). Moreover, although the ship track of leg II covered large areas with higher

335 chlorophyll-a concentrations, ~~but~~ the high EF_{Ca} values were only present at the narrow temporal
336 and spatial scales. Furthermore, results from back trajectories indicated that air masses did not
337 significantly travel through the region with elevated chlorophyll-a concentration. Therefore, we
338 suggest that the impact of chlorophyll-a concentration ~~may have a limited impact~~ on Ca^{2+}
339 enrichment may be limited.

340 3.2 Single-particle characteristics of Ca-containing particles

341 To elucidate the mixing state of individual calcareous particles, we set a threshold of m/z 40
342 $[Ca]^+$ to reclassify all ~~the~~ single-particle types that were obtained from the ART-2a algorithm. This
343 means that all reclassified particles contain signals of m/z 40 $[Ca]^+$. ~~were further refined with an~~
344 ~~ion signal of m/z 40 $[Ca]^+$.~~ A total of ~ 580, 000 Ca-containing particles were distributed among
345 all particle types, accounting for ~ 62% of the total obtained particles. ~~In particular,~~ OC-Ca was
346 the dominant (~ 72%, by occurrence frequency) particle type among all Ca-containing particles,
347 followed by SS-Ca (calcium-containing sea salt, ~ 12%) (**Fig. 36h**). Each of the remaining particle
348 types accounted for negligible fractions (< 7%) in the total of Ca-containing particles, and were
349 classified as “Other”. ~~Thus, they are~~ they were not included in the following discussion.

350 OC-Ca ~~is~~ was characterized by a prominent ion signature for m/z at 40 $[Ca]^+$ in the positive
351 mass spectrum and organic marker ions of biological origin (e.g., organic nitrogen, phosphate,
352 carbohydrate, siliceous materials, and organic carbon) in the negative spectrum (**Fig. 36d**).
353 Specifically, organic nitrogen (m/z -26 $[CN]^-$ and -42 $[CNO]^-$) ~~shows~~ showed the largest number
354 fraction (NF) at ~88% (**Fig. S5h**), which is likely derived from organic nitrogen species, such as
355 amines amino groups, and/or cellulose (Czerwieniec et al., 2005; Srivastava et al., 2005; Köllner

356 et al., 2017; Dall'osto et al., 2019). Higher NFs of phosphate (16%; m/z -63 $[\text{PO}_2]^-$ and -79 $[\text{PO}_3]^-$),
357 carbohydrates (24%; m/z -45 $[\text{CHO}_2]^-$, -59 $[\text{C}_2\text{H}_3\text{O}_2]^-$, and -73 $[\text{C}_3\text{H}_5\text{O}_2]^-$), siliceous materials
358 (40%; m/z -60 $[\text{SiO}_2]^-$), and organic carbon (37%; m/z 27 $[\text{C}_2\text{H}_3]^-$ and 43 $[\text{C}_2\text{H}_3\text{O}_3]^-$) were also
359 observed in OC-Ca relative to other particle types (**Fig. S5h**). These organic ion signatures likely
360 correspond to phospholipids, mono- and polysaccharides, and biosilica structures (e.g.,
361 exoskeletons or frustules), which may be derived from the intact heterotrophic cells, fragments of
362 cells, and exudates of phytoplankton and/or bacterial (Prather et al., 2013; Guasco et al., 2014;
363 Zhang et al., 2018). Besides, the strong organic ion intensities may truly reflect the amount of
364 organic material in OC-Ca, because the particles ~~were~~are sufficiently dry during the ionization
365 process (i.e., complete positive and negative mass spectra) (Gross et al., 2000). Notably, the
366 possible ion signals of bromide (m/z -79 and -81) were observed in OC-Ca, indicating a potential
367 source of blowing snow (Yang et al., 2008; Song et al., 2022).

368 The OC-Ca particles ~~were~~are most likely classified as a distinct **SSASSAs** population,
369 probably of marine biogenic origin. Sea salt particles typically exhibit a stronger m/z 23 $[\text{Na}]^+$ than
370 m/z 40 $[\text{Ca}]^+$ due to the higher concentration of Na^+ vs. Ca^{2+} in seawater and also due to the lower
371 ionization potential of Na vs. Ca (5.14 eV vs. 6.11 eV) (Gross et al., 2000). However, the ratio of
372 m/z 23 $[\text{Na}]^+$ to m/z 40 $[\text{Ca}]^+$ ~~present~~ in the OC-Ca particles is reversed, verifying a distinct single
373 particle type (Gross et al., 2000; Gaston et al., 2011). Similarly, the ion signal of m/z 39 $[\text{K}]^+$ does
374 not surpass that of m/z 40 $[\text{Ca}]^+$ in OC-Ca, although K is ionized more easily ~~than~~ Ca (4.34 eV vs.
375 6.11eV) (Gross et al., 2000). ~~The presence of calcium together with organic species (e.g., organic~~
376 ~~nitrogen, phosphate, etc.) in SSA verifies a marine biogenic origin of OC-Ca (Köllner et al., 2021).~~
377 Although RH at the sampling outlet was < 40%, the short residence time of the particles within the

378 drying tube (< 5 s) and vacuum system (< 1 ms) could have been insufficient for the complete
379 efflorescence of SSASSAs (Gaston et al., 2011; Sierau et al., 2014). Hence, the OC-Ca could not
380 be attributed to the chemical fractionation of the efflorescence SSASSAs in SPAMS analysis.
381 Additionally, based on the single-particle mass spectrometry technique, some particle types with
382 similar chemical characteristics to OC-Ca have been observed in both field and laboratory studies
383 (e.g., atomization of sea ice meltwater collected in the Southern Ocean) (Gaston et al., 2011;
384 Prather et al., 2013; Collins et al., 2014; Guasco et al., 2014; Dall'osto et al., 2019; Su et al., 2021).
385 The OC-Ca may be from local emissions because the measurements were almost entirely
386 influenced by polar air masses (Fig. S1). Other possible sources, such as glacial dust (Tobo et al.,
387 2019), could be excluded because of the lack of crustal mass spectral characteristics (e.g., -76
388 $[\text{SiO}_3]^-$, 27 $[\text{Al}]^+$, and 48 $[\text{Ti}]^+/64 [\text{TiO}]^+$) (Pratt et al., 2009; Zawadowicz et al., 2017). And tThe
389 mean mass concentration ratio of Ca/Na in the aerosol sample was only 0.10, much lower than
390 that in the crust (1.78, w/w).

391 In contrast, SS-Ca was classified as a pure inorganic cluster with predominant contributions
392 of Na-related compounds (m/z 23 $[\text{Na}]^+$, 46 $[\text{Na}_2]^+$, 81/83 $[\text{Na}_2^{35/37}\text{Cl}]^+$, and -93/-95 $[\text{Na}^{35/37}\text{Cl}_2]^-$),
393 Mg (m/z 24), K (m/z 39), and Ca (m/z 40) in the mass spectra (**Fig. 6a3**). Organic ion signals such
394 as organic nitrogen (m/z -26 $[\text{CN}]^-$ and -42 $[\text{CNO}]^-$) and phosphate (m/z -63 $[\text{PO}_2]^-$ and -79 $[\text{PO}_3]^-$)
395 were rarely detected (~1%, by NF). As described above, These compounds related to oceanic
396 biogeochemical processes. In addition, secondary species (e.g., nitrate of m/z -62 $[\text{NO}_3]^-$ and
397 sulfate of m/z -97 $[\text{HSO}_4]^-$) were also not observed, indicating a fresh origin and/or less
398 atmospheric aging. As a subpopulation of SS, SS-Ca may originate from bubble bursting within
399 open -water and/or blowing snow.

400 4 Discussion

401 SS-Ca (calcium-containing sea salt) represents a mixture of NaCl and CaCl₂. However, the
402 SS-Ca showed a weak correlation ($r = 0.21, p < 0.05$, by count and $r = 0.03, p < 0.05$, by the peak
403 area of m/z 40 [Ca]⁺) with the mass concentration of Ca²⁺ (**Table S51**). In addition, the proportion
404 of SS-Ca ~~is-was~~ also small (11.6%, **Fig. 6h**). These results indicated that CaCl₂ is not the major
405 ~~cause-reason for~~ the Ca²⁺ enrichment in **SSASSAs**, although CaCl₂ has been proposed as a cause,
406 based on laboratory atomizing of pure inorganic artificial seawater (Salter et al., 2016). The
407 contribution of ikaite (CaCO₃·6H₂O) could also be excluded due to its low water solubility
408 (Bischoff et al., 1993; Dieckmann et al., 2008; Dieckmann et al., 2010), although ikaite from sea
409 salt fractionation has also been proposed to account for the Ca²⁺ enrichment in ~~the~~ **SSASSAs** over
410 the Antarctic coast (Hara et al., 2012). Moreover, the mass spectral signatures of CaCO₃ (e.g., m/z
411 56 [CaO]⁺ and -60 [CO₃]²⁻ (see Sullivan et al. (2009)) were also rare in the SS-Ca particles (**Fig.**
412 **6a3**).

413 As a major component (~ 72%, by occurrence frequency) of the Ca-containing particles, OC-
414 Ca ~~was-is~~ expected to be partially responsible for the calcium enrichment in **SSASSAs**. First,
415 the OC-Ca and mass concentration of Ca²⁺ exhibited moderately weak positive correlations ($r =$
416 $0.42, p < 0.05$, by count and $r = 0.49, p < 0.05$, by the peak area of m/z 40 [Ca]⁺) (**Table S5**) and
417 moderately strong correlations under higher EF_{Ca} values (EF_{Ca} > 10, $r = 0.63, p < 0.05$, by count
418 and $r = 0.68, p < 0.05$, by the peak area of m/z 40 [Ca]⁺) (**Table S5 and SI text S6**). Also, such
419 correlations were great during leg I ($r = 0.59, p < 0.05$, by count and $r = 0.60, p < 0.05$, by the
420 peak area of m/z 40 [Ca]⁺). -Second, the OC-Ca showed a size distribution with a peak at 1 μm
421 (**Fig. 36j**), which is consistent with the significant Ca²⁺ enrichment that is generally found in

422 submicron ~~SSASSAs~~ (Cochran et al., 2016; Salter et al., 2016; Mukherjee et al., 2020).

423 We further show that calcium may strongly mix with organic matter, probably as organically
424 complexed calcium, in the OC-Ca particles. The calcium ~~was well~~-correlated well with different
425 kinds of organic matter (e.g., phosphate, $r = 0.81$, $p < 0.05$, by peak area), but poorly correlated
426 with chloride ($r = 0.21$, $p < 0.05$, by the peak area and $r = 0.48$, $p < 0.05$, by mass concentration)
427 (**Fig. S69**). In addition, different kinds of organic matter (e.g., organic nitrogen, organic carbon,
428 etc.) in the OC-Ca particles also showed enrichment trends below the submicron level,
429 analogously to Ca^{2+} enrichment (**Fig. S810**). Particularly, EF_{Ca} and organic nitrogen (with the
430 largest NF in OC-Ca) were both affected by the environmental factors of ambient temperature,
431 wind speed, and sea ice fraction, indicating possible organic binding with calcium (**Fig. S944**).

432 To exclude the potential inorganic water-soluble compounds (i.e., chloride (m/z -35 and -37),
433 nitrate (m/z -62), and sulfate (m/z -97)), we further classified OC-Ca into two subpopulations, OC-
434 Ca-Organic (23.6%, by proportion) and OC-Ca-Inorganic (48.7%, by proportion) (**Fig. S12S10**),
435 depending on the presence of inorganic ion signals (i.e., chloride of m/z -35/-37 [Cl^-], nitrate of
436 m/z -62 [NO_3^-], and sulfate of m/z -97 [HSO_4^-]). Both the OC-Ca types and mass concentrations of
437 Ca^{2+} showed enhanced correlations under high EF_{Ca} values (**Table S51**). In particular, OC-Ca-
438 Organic exhibited stronger correlations than did OC-Ca-Inorganic ($r = 0.51$ vs. $r = 0.28$, $p < 0.05$,
439 by count and $r = 0.51$ vs. 0.31 , $p < 0.05$, by peak area of m/z 40 [Ca^+], respectively), which
440 ~~indicated~~ indicates the importance of OC-Ca-Organic for the enrichment of Ca^{2+} . Although we did
441 not measure the hygroscopicity of the OC-Ca in this study, we infer it to be hygroscopic to some
442 extent. As reported by Cochran et al. (2017), the mixture of sea salt with organic matter can also
443 exhibit a certain hygroscopicity (hygroscopicity parameter, 0.50-1.27). Therefore, it is likely that

444 ~~the organically complexed calcium is slightly water-soluble and is partially responsible for~~
445 ~~calcium enrichment, while current studies may neglect it. Therefore, the organically complexed~~
446 ~~calcium was most likely water insoluble and/or slightly water-soluble and partly responsible for~~
447 ~~calcium enrichment, while current studies may neglect it.~~

448 The possible processes contributing to the calcium enrichment induced by OC-Ca ~~are~~
449 ~~illustrated in~~ can only be speculated on (Fig. 47). Ca^{2+} tends to bind with organic matter of
450 biogenic origin, such as exopolymer substances (EPSs), and subsequently assemble as marine
451 microgels (Verdugo et al., 2004; Gaston et al., 2011; Krembs et al., 2011; Orellana et al., 2011;
452 Verdugo, 2012; Orellana et al., 2021). Large amounts of microgels, driven by sea ice algae,
453 microorganisms, and/or exchanges of organic matter with the seawater below, stick to the sea ice
454 due to its porous nature. And they are likely to present in the snow, frost flowers, and brine
455 channels. Due to its porous nature, the sea ice sticks to the abundant microgels that are driven by
456 sea ice algae, microorganisms, and/or exchanges of organic matter with the seawater below, which
457 are likely present in the snow, frost flowers, and brine channels (Krembs et al., 2002; Gao et al.,
458 2012; Vancoppenolle et al., 2013; Arrigo, 2014; Boetius et al., 2015; Kirpes et al., 2019). A low
459 wind speed may not only be conducive to the formation of frost flowers and snow but also
460 produce less sea salt (i.e., small yields of Na^+ relative to Ca^{2+}) (Rankin et al., 2002).
461 Correspondingly, a high wind speed ($\geq 7 \text{ m s}^{-1}$) can yields more sea salt by blowing-snow events
462 and/or wave breaking (Yang et al., 2008; Song et al., 2022), presenting a dilution effect of Na^+ on
463 Ca^{2+} . In this case, the calcium enrichment in SSASSAs could reasonably be attributed to the
464 possible gel-like calcium-containing particles released by low-wind-blown sea ice.~~the gel-like~~
465 ~~calcium particles~~ This inference is supported by the observation of air masses blown over a large

466 fraction of sea ice/ land-based Antarctic ice, as well as a moderate negative correlation ($r = 0.50$, p
467 < 0.001) between wind speed and sea ice fraction. In addition, we also observed a (higher
468 proportion of OC-Ca at low wind speeds ($< 7 \text{ m s}^{-1}$, 61.5%) ~~than relative to~~ high wind speeds (\geq
469 7 m s^{-1} , 38.5%)). Coincidentally, Song et al. (2022) also reported that a low wind-blown sea ice
470 process can drive the biogenic aerosol response in the high Arctic ~~area~~. In addition, the enhanced
471 presence of film drops was observed at lower wind speeds ($< 6 \text{ m s}^{-1}$) (Norris et al., 2011), which
472 suggests that the bubble bursts within the sea ice leads and open water may also be responsible
473 for the release of OC-Ca and its calcium enrichment involved (Leck and Bigg, 2005b, a; Bigg and
474 Leck, 2008; Leck and Bigg, 2010; Leck et al., 2013; Kirpes et al., 2019).

475 As expected, the results of the Ca^{2+} enrichment in SSAs obtained from ion mass
476 concentration via IGAC did not fully align with results from SPAMS datasets. We propose two
477 possible explanations for this discrepancy: (i) It could be attributed to a difference in the size of
478 particles collected by the two different instruments ($\sim 10 \mu\text{m}$ for IGAC and $0.2\text{--}2 \mu\text{m}$ for SPAMS).
479 In addition, SPAMS cannot measure the Aitken-mode particles (Sierau et al., 2014), and can
480 measure only the tail of accumulation-mode particles with a relatively low hit rate ($\sim 11\%$ in this
481 study). (ii) The types of datasets obtained via IGAC (ion mass concentration) and SPAMS (mass
482 spectral characteristics) are different. The former method partially reflects the Ca^{2+} distribution
483 based on water-soluble Ca^{2+} , while the OC-Ca measured by SPAMS may have low water
484 solubility. The latter method is still challenging to use for quantitative measurements due to
485 potential inhomogeneities in the transmission efficiencies of the aerodynamic lenses and
486 desorption/ionization, as well as the matrix effects of individual particles ~~due to the potential~~
487 ~~inhomogeneities in the transmission efficiencies of the aerodynamic lenses and~~

488 desorption/ionization, and the matrix effects of individual particles-(Gross et al., 2000; Qin et al.,
489 2006; Pratt and Prather, 2012). Therefore, it may not be straightforward to compare the particle
490 count and peak area with the absolute mass concentration.~~use the particle count and peak area in~~
491 ~~comparison with the absolute mass concentration.~~

492 Although there is a discrepancy between the two instruments, we believe our results to be
493 reliable and representative. On the one side, the quantitative results concluded by IGAC confirm
494 the enrichment of Ca²⁺ in SSAs and demonstrate their dependence on and relevance to the
495 environmental factors. On the other side, the individual particle analysis ranging in size from 0.2
496 to 2 μm is highly appropriate for revealing the calcium distribution in SSAs, as previous studies
497 have shown increasing Ca²⁺ enrichment in SSAs below 1 μm (Oppo et al., 1999; Hara et al., 2012;
498 Cochran et al., 2016; Salter et al., 2016; Mukherjee et al., 2020). Our study successfully identifies
499 a unique calcareous particle type (i.e., OC-Ca) and its specific mixing state. A comprehensive
500 understanding of the characteristics of OC-Ca to the mechanisms of calcium enrichment is
501 essential for further recognizing the CCN and IN activation in remote marine areas.

502 Another limitation is that only several environmental factors were considered for calcium
503 enrichment in this study. Some potential factors, such as surface net solar radiation, snowfall, total
504 cloud cover, surface pressure, total precipitation, boundary layer height, seawater salinity, etc.,
505 may also affect the calcium enrichment in SSAs through regulating the yield of sea salt (i.e., Na⁺
506 mass concentration)(Song et al., 2022). However, they were not available in this study because of
507 the lack of measurement during the cruise. Meanwhile, the satellite data with low temporal-spatial
508 resolution cannot match per hour in each starting condition. We hope that future research will
509 further investigate the enrichment of specific species in SSAs under a wider range of

510 meteorological or oceanographic conditions.

511 Noticeable, it is still quite a challenge to obtain quantitative measurements using SPAMS due
512 to the potential inhomogeneities in the transmission efficiencies of the aerodynamic lenses and
513 desorption/ionization, and the matrix effects of individual particles (Gross et al., 2000; Qin et al.,
514 2006; Pratt and Prather, 2012). SPAMS cannot measure the Aitken mode particles (Sierau et al.,
515 2014), it can measure only the tail of accumulation mode particles with relatively low hit rate (~11%
516 in this study). Additionally, there is a difference in the size of collected particles between SPAMS
517 (0.2–2 µm) and IGAC (~10 µm). Meanwhile, IGAC may partly reflect the Ca²⁺ distribution based
518 the water-soluble Ca²⁺ as OC-Ca may have a low water solubility. Therefore, it may not be
519 straightforward to use the particle count and peak area in comparison with the absolute mass
520 concentration. Nevertheless, our results successfully identified a unique calcareous particle type
521 (i.e., OC-Ca) and its specific mixing state, which provides some insights into the mechanisms
522 behind calcium enrichment.

523 **5 Conclusions and atmospheric implications**

524 We investigated the distribution of calcium in SSASSAs through the R/V *Xuelong* cruise
525 observation campaigns over the Ross Sea, Antarctica. The most significant Ca²⁺ enrichment in
526 SSASSAs occurred under relatively lower ambient temperatures (< -3.5 °C) and wind speeds (< 7
527 m s⁻¹) and with the presence of sea ice. With the help of individual particle mass spectral analysis,
528 we first proposed that a single-particle type of OC-Ca (internally mixed organics with calcium),
529 probably resulting from the preferential binding of Ca²⁺ with organic matter, could partially
530 account for the calcium enrichment in SSASSA. We speculate ~~inferred~~ that OC-Ca is likely

531 produced from the effects of low wind-blown sea ice on microgels induced by Ca^{2+} and/or the
532 bubble bursts in the open-water and/or sea ice leads. However, the impact of environmental
533 factors and OC-Ca on calcium enrichment in SSASSA still cannot be well predicted by multiple
534 linear regression and random forest analysis (SI text S57), which may be ascribed to other
535 unknown mechanisms and/or organically complexed calcium with a low water solubility. In
536 addition, our conclusions based on limited spatial, ~~and~~ temporal, meteorological, and
537 oceanographic conditions may not be accessible to other seasons and oceanic basins.

538 We suggest that the environmental behaviors of the possible gel-like calcium-containing
539 particles (i.e., OC-Ca) should be paid more attention behind the mechanisms of calcium
540 enrichment. Under the stimulation of specific environmental factors (e.g., pH, temperature,
541 chemical compounds, pollutants, and UV radiation), their physicochemical properties would be
542 changed (e.g., water-solubility enhanced by the cleavage of polymers) (Orellana and Verdugo,
543 2003; Orellana et al., 2011).~~To our knowledge, this is the first report of a calcium dominated~~
544 ~~single-particle type OC-Ca in the Antarctic.~~ Such particles may be preferred candidates for CCN
545 and/or IN (Willis et al., 2018; Lawler et al., 2021). To our knowledge, this is the first report of a
546 calcium-dominated single-particle type OC-Ca in the Antarctic. In the context of global warming
547 and sea ice retreat, this work provides insight into the chemical composition and distribution of
548 submicron SSASSAs in the Antarctic summer atmosphere, which would be helpful for a better
549 understanding of aerosol-cloud-climate interactions.

550 **Data Availability Statement**

551 The data are available at Zenodo (<https://doi.org/10.5281/zenodo.7276073>). Details can be

552 [accessed by contacting the corresponding author Guohua Zhang \(zhanggh@gig.ac.cn\) and the first](#)
553 [author Bojiang Su \(subojiang21@mails.ucas.ac.cn\).](#)

554 **Declaration of Competing Interest**

555 The authors declare that they have no known competing financial interests or personal
556 relationships that could have appeared to influence the work reported in this paper.

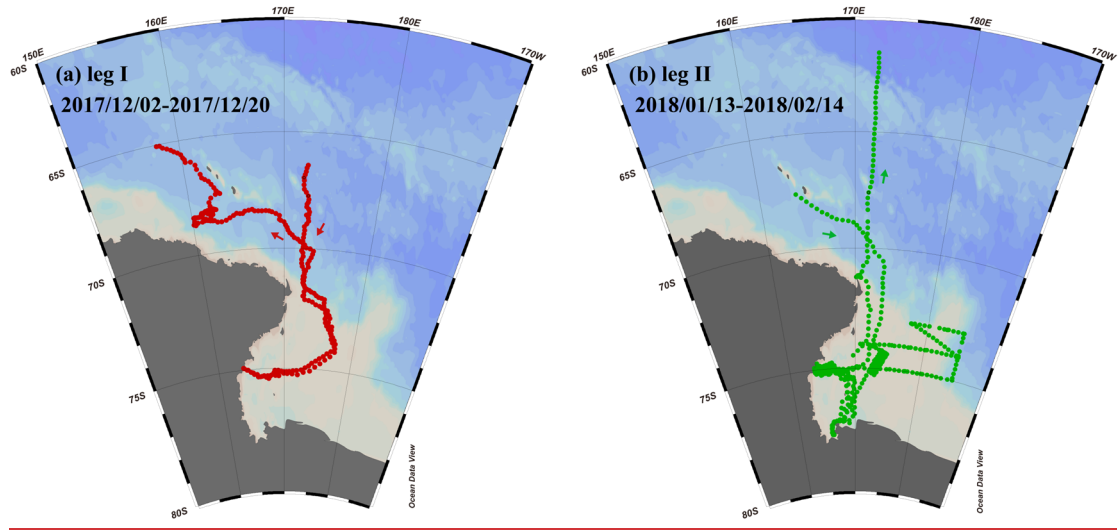
557 **Author Contributions**

558 The idea for the study was conceived by BJS. BJS analyzed the data, prepared the figures, and
559 wrote the manuscript under the guidance of GHZ and XYB. LL and JPY contributed to the
560 observation data. All co-authors contributed to the discussions of the results and refinement of the
561 manuscript.

562 **Acknowledgment**

563 This work was supported by the Guangdong Basic and Applied Basic Research Foundation
564 (2019B151502022), the National Natural Science Foundation of China (42077322 and 42130611),
565 the Youth Innovation Promotion Association CAS (2021354), and the Guangdong Foundation for
566 Program of Science and Technology Research (2020B1212060053). [The authors would like to](#)
567 [thank the editor and reviewers for their valuable time and feedback.](#)

568 **Figure captions**



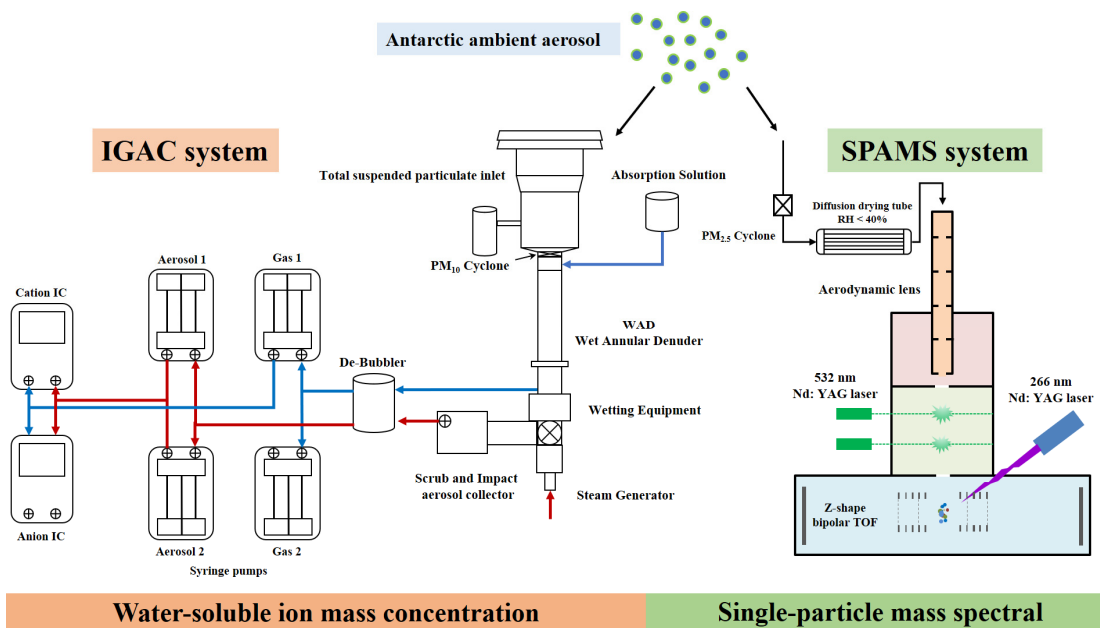
569

570 **Figure 1**

571 Observation campaigns through R/V *Xuelong* in the Ross Sea, Antarctic. (a) Leg I took place from

572 December 2-20, 2017. (b) Leg II was conducted from January 13 to February 14, 2018.

573



Water-soluble ion mass concentration

Single-particle mass spectral

574

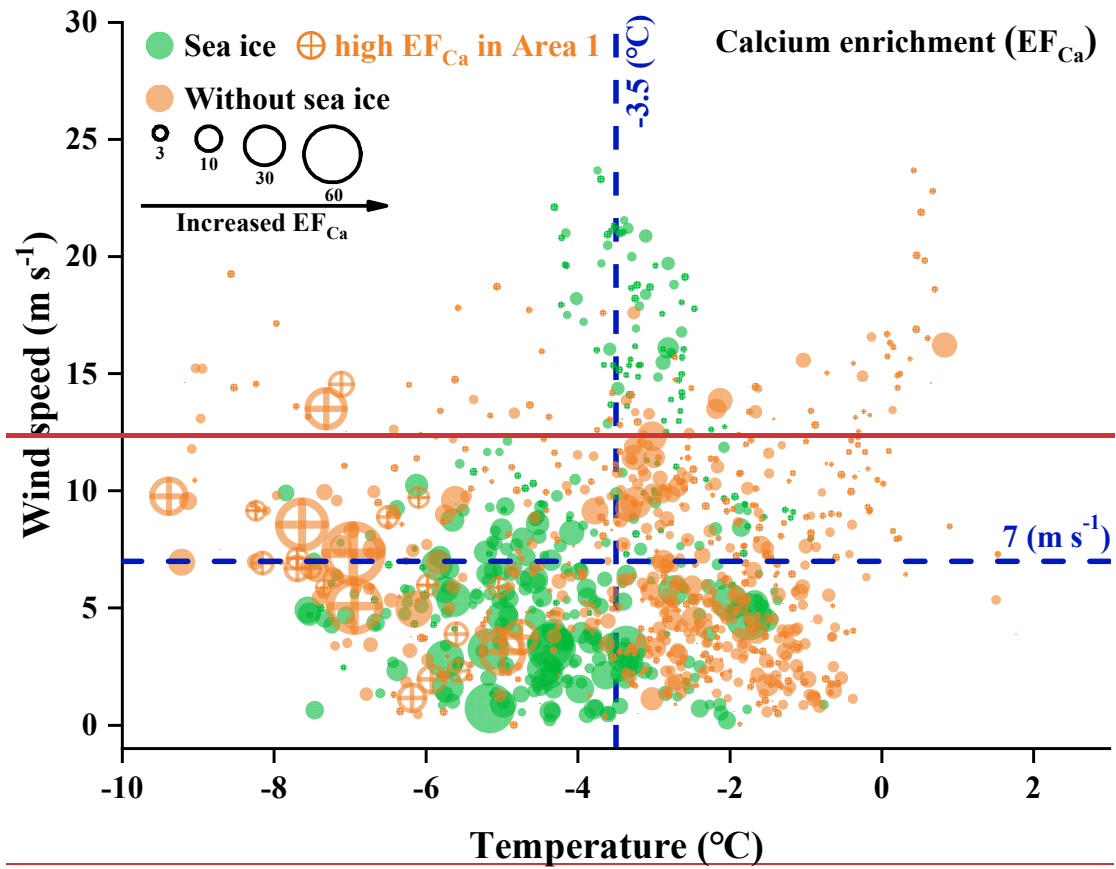
575 **Figure 2**

576 A schematic of the aerosol sampling system of IGAC and SPAMS during the research cruise over

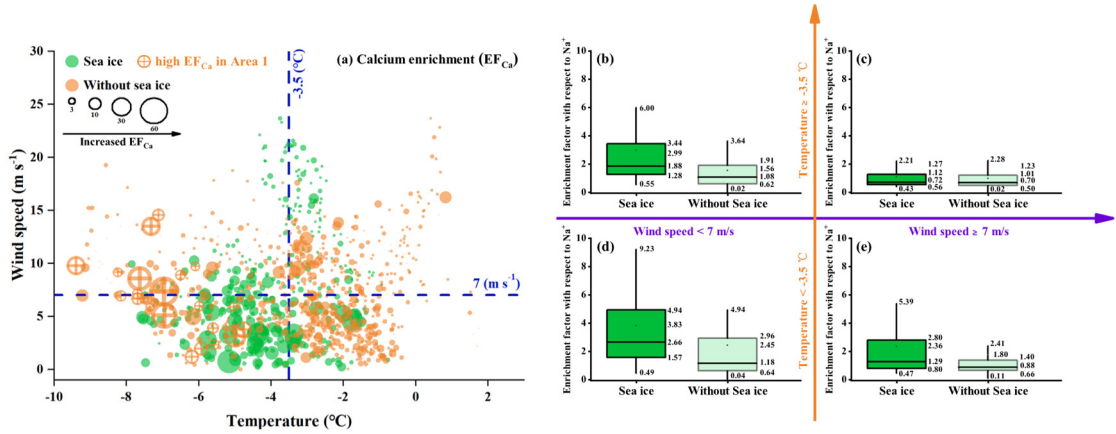
577 the Ross Sea, Antarctic.

578

579
580



581



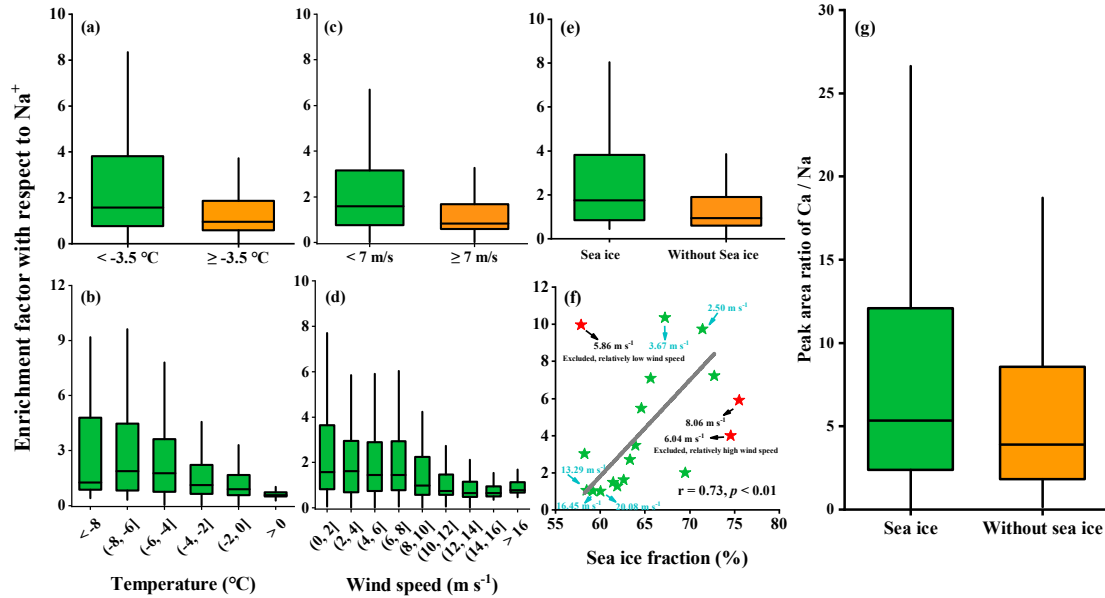
582

583 **Figure 31**

584 (a) Bubble chart of the hourly Ca^{2+} enrichment factor (EF_{Ca}) with respect to Na^{+} with different
585 environmental factors (ambient temperature, wind speed, and sea ice fraction). The green and
586 orange dots represent the EF_{Ca} values for the periods with and without sea ice, respectively. The

587 orange marked dots represent a series of high EF_{Ca} cases that were correlated with a high
588 concentration of chlorophyll-a during leg II of the cruise. (b)-(e) Data support of the bubble chart
589 represented by box and whisker plots. In the box and whisker plots, the marked values from top to
590 bottom are the 90th and 75th percentiles, mean, median, and 25th and 10th percentiles,
591 respectively.

592

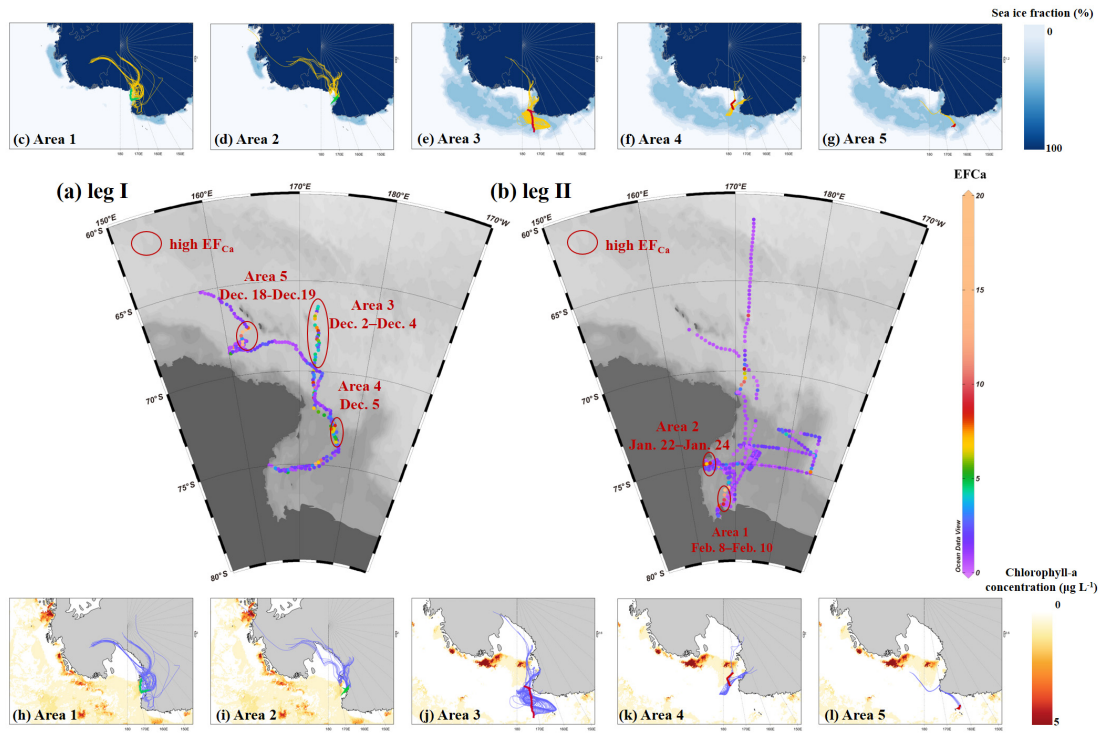


593

594 **Figure 42**

595 Enrichment factors of Ca^{2+} with respect to Na^+ varied as a function of the ambient temperature (a-
 596 b), wind speed (c-d), and sea ice fraction (e-f) during cruise observation campaigns. (g) A box and
 597 whisker plot of the single-particle peak area ratio of Ca/Na in OC-Ca for the periods with and
 598 without sea ice. In the box and whisker plots, the lower, median, and upper lines of the box denote
 599 the 25th, 50th, and 75th percentiles, respectively. The lower and upper edges denote the 10th and
 600 90th percentiles, respectively. The black solid star (f) exhibited an anomalous trend due to its
 601 nature of ~~the~~ relatively high or low wind speed. The first point exhibited a high EF value because
 602 of its relatively low wind speed (5.86 m s^{-1}). The second and third points exhibited low EF values
 603 because of their relatively high wind speeds of 6.04 m s^{-1} and 8.06 m s^{-1} , respectively. These three
 604 points have been excluded ~~from~~ the correlation analysis.

605

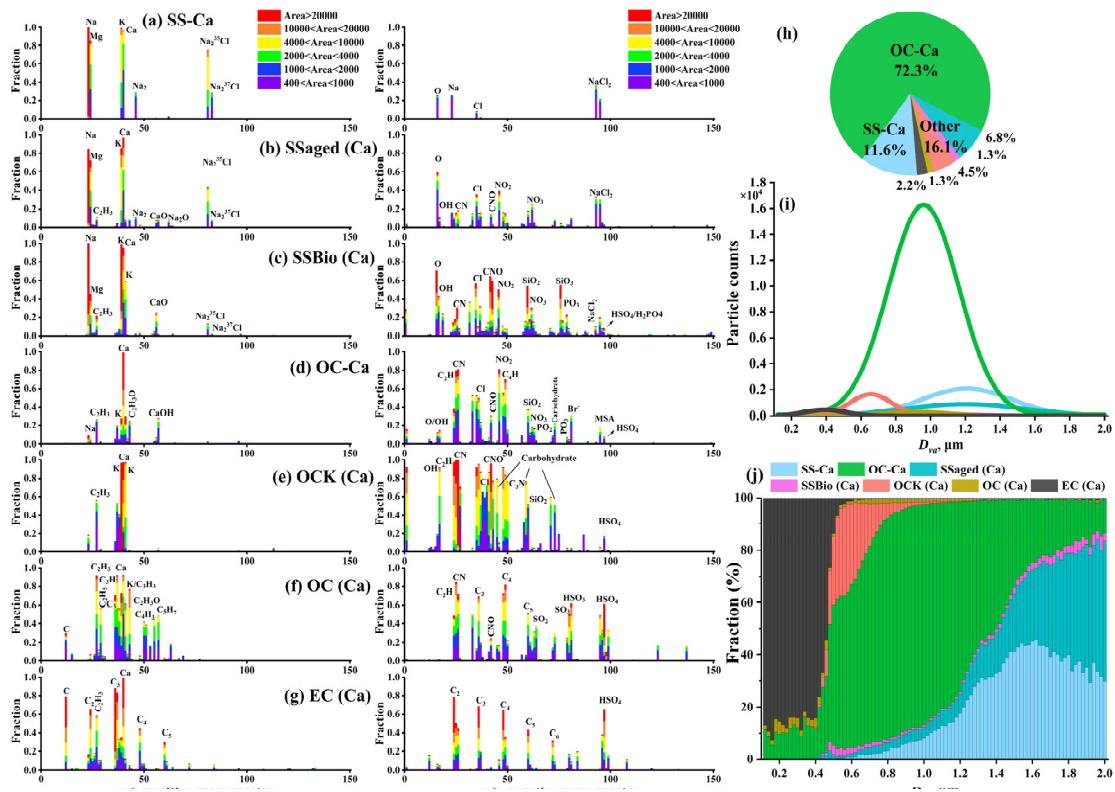
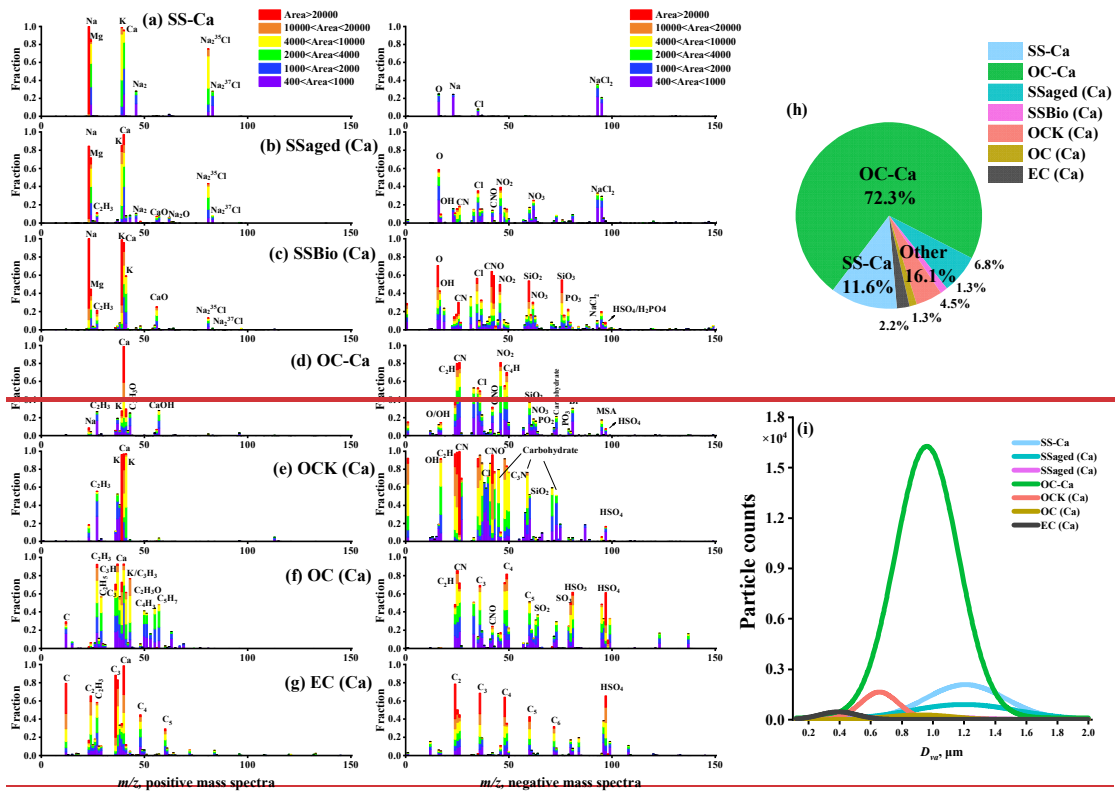


606

607 **Figure 5**

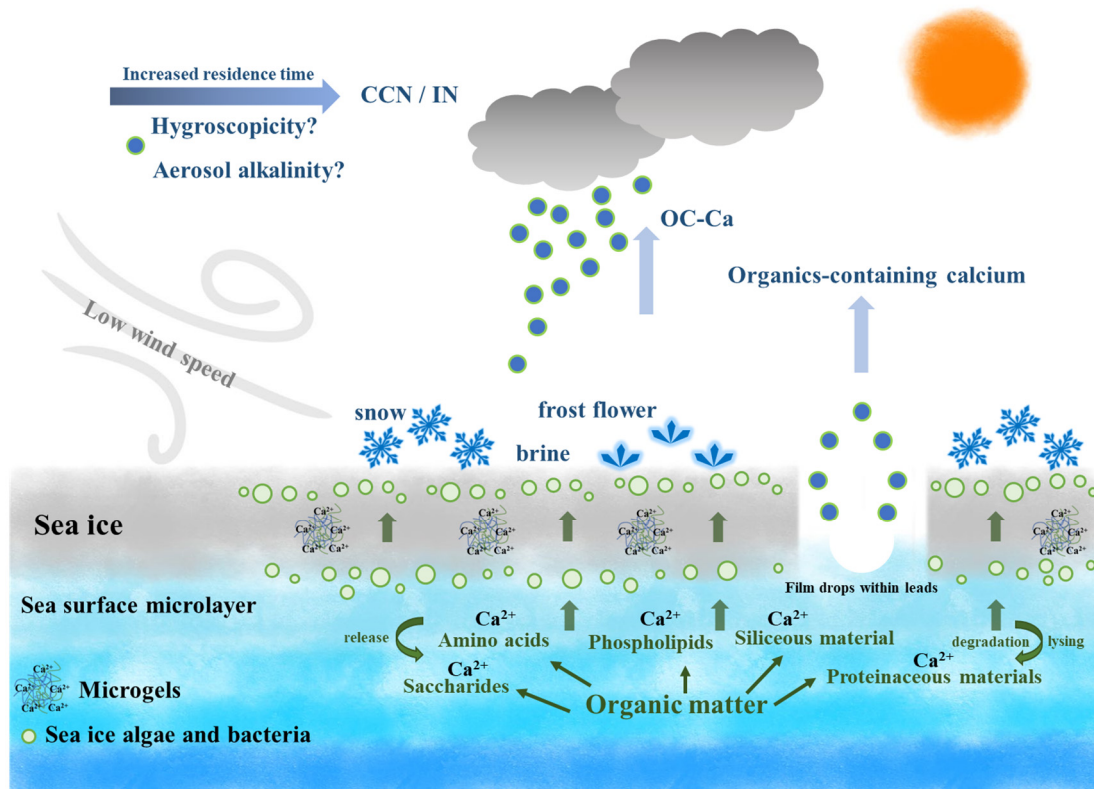
608 Distribution of EF_{Ca} during (a) leg I and (b) leg II. Five distinct areas with continuous enhanced
 609 Ca^{2+} enrichment events, along with 96-hour back trajectories (one trajectory per hour in each
 610 starting condition), sea ice fraction (c-g, yellow traces), and chlorophyll-a concentration (h-l, light-
 611 blue traces). Lines in red and green referred to ship tracks for corresponding areas during the leg I
 612 and leg II, respectively.

613



617 **Figure 36**

618 (a) – (g) Average digitized single-particle mass spectra of seven chemical classes of Ca-containing
619 particles. New single-particle types are reclassified with m/z 40 $[Ca^{2+}]$ based on previous ART-2a
620 results. (h) Relative proportion and (i) unscaled size-resolved number distributions of ~~these~~ single-
621 particle types using Gaussian Fitting. (j) Number fractions of single-particle types per size bin
622 versus particle size.



623

624 **Figure 47**

625 Schematic of the production of OC-Ca and its possible atmospheric implications beyond calcium
 626 enrichment. Ca²⁺ tends to bind with organic matter whining sea ice/seawater, and subsequently
 627 assemble to marine microgels, likely present in the snow, frost flowers, and brine channels. With
 628 the low wind-blown sea ice process and/or bubble bursting within sea ice leads, these gel-like
 629 particles (i.e., OC-Ca) may be released to the Antarctic atmosphere, as a potential source of
 630 CCN/IN. Notably, the dataset via SPAMS cannot directly identify marine microgels. OC-Ca was
 631 likely associated with marine microgels, as calcium and biological organic material were
 632 extensively internally mixed. This OC-Ca type has previously been observed in the laboratory
 633 simulation of (Collins et al., 2014).

634 **Table captions**

EF _{Ca}	Count (Correlation coefficient, r)				Peak area (Correlation coefficient, r, m/z 40 [Ca] ²⁺)			
	OC-Ca-Inorganic	OC-Ca-Organic	OC-Ca	SS-Ca	OC-Ca-Inorganic	OC-Ca-Organic	OC-Ca	SS-Ca
0 - 5	0.08	0.31	0.18	0.07	0.18	0.44	0.41	0.04
5 - 10	0.15	0.37	0.27	0.04	0.14	0.36	0.33	0.06
> 10	0.58	0.59	0.63	0.10 ^a	0.53	0.68	0.68	0.10
Leg I	0.45	0.59	0.55	0.02	0.53	0.60	0.60	0.03
Leg II	0.06	0.22	0.14	0.45	0.14	0.39	0.39	0.11
Total	0.28	0.51	0.42	0.21	0.31	0.51	0.49	0.03

a: p-value > 0.05
(Pearson method, two-tailed test)

635
636 **Table 1**

637 **Correlation analysis between the OC-Ca (by count and by the peak area of m/z 40 [Ca]⁺) and its**
638 **two subpopulations OC-Ca-Organic and OC-Ca-Inorganic, SS-Ca (by count and by the peak area**
639 **of m/z 40 [Ca]⁺), and mass concentration of Ca²⁺ in the variation of EF_{Ca}, with the p-value < 0.05.**

640
641 **References**

- 642 Arrigo, K. R.: Sea ice ecosystems, *Ann Rev Mar Sci*, 6, 439-467, [https://doi.org/10.1146/annurev-](https://doi.org/10.1146/annurev-marine-010213-135103)
643 [marine-010213-135103](https://doi.org/10.1146/annurev-marine-010213-135103), 2014.
- 644 Bertram, T. H., Cochran, R. E., Grassian, V. H., and Stone, E. A.: Sea spray aerosol chemical
645 composition: elemental and molecular mimics for laboratory studies of heterogeneous and
646 multiphase reactions, *Chemical Society Reviews*, 47, 2374-2400,
647 <https://doi.org/10.1039/c7cs00008a>, 2018.
- 648 Bigg, E. K. and Leck, C.: The composition of fragments of bubbles bursting at the ocean surface,
649 *Journal of Geophysical Research: Atmospheres*, 113 <https://doi.org/10.1029/2007jd009078>, 2008.
- 650 Bischoff, J. L., Fitzpatrick, J. A., and Rosenbauer, R. J.: The Solubility and Stabilization of Ikaite
651 (CaCO₃·6H₂O) from 0-Degrees-C To 25-Degrees-C - Environmental and Paleoclimatic Implications
652 for Thiolite Tufa, *J Geol*, 101, 21-33, <https://doi.org/10.1086/648194>, 1993.
- 653 Boetius, A., Anesio, A. M., Deming, J. W., Mikucki, J. A., and Rapp, J. Z.: Microbial ecology of the
654 cryosphere: sea ice and glacial habitats, *Nat Rev Microbiol*, 13, 677-690,
655 <https://doi.org/10.1038/nrmicro3522>, 2015.
- 656 Boreddy, S. K. R. and Kawamura, K.: A 12-year observation of water-soluble ions in TSP aerosols
657 collected at a remote marine location in the western North Pacific: an outflow region of Asian dust,
658 *Atmos Chem Phys*, 15, 6437-6453, <https://doi.org/10.5194/acp-15-6437-2015>, 2015.
- 659 Brooks, S. D. and Thornton, D. C. O.: Marine Aerosols and Clouds, *Annu Rev Mar Sci*, 10, 289-313,
660 <https://doi.org/10.1146/annurev-marine-121916-063148>, 2018.

661 Carter-Fenk, K. A., Dommer, A. C., Fiamingo, M. E., Kim, J., Amaro, R. E., and Allen, H. C.: Calcium
662 bridging drives polysaccharide co-adsorption to a proxy sea surface microlayer, *Phys Chem Chem*
663 *Phys*, 23, 16401-16416, <https://doi.org/10.1039/d1cp01407b>, 2021.

664 Chi, J. W., Li, W. J., Zhang, D. Z., Zhang, J. C., Lin, Y. T., Shen, X. J., Sun, J. Y., Chen, J. M., Zhang, X.
665 Y., Zhang, Y. M., and Wang, W. X.: Sea salt aerosols as a reactive surface for inorganic and organic
666 acidic gases in the Arctic troposphere, *Atmos Chem Phys*, 15, 11341-11353,
667 <https://doi.org/10.5194/acp-15-11341-2015>, 2015.

668 Cochran, R. E., Jayarathne, T., Stone, E. A., and Grassian, V. H.: Selectivity Across the Interface: A
669 Test of Surface Activity in the Composition of Organic-Enriched Aerosols from Bubble Bursting, *J*
670 *Phys Chem Lett*, 7, 1692-1696, <https://doi.org/10.1021/acs.jpcllett.6b00489>, 2016.

671 Cochran, R. E., Laskina, O., Trueblood, J. V., Estillore, A. D., Morris, H. S., Jayarathne, T., Sultana, C.
672 M., Lee, C., Lin, P., Laskin, J., Laskin, A., Dowling, J. A., Qin, Z., Cappa, C. D., Bertram, T. H.,
673 Tivanski, A. V., Stone, E. A., Prather, K. A., and Grassian, V. H.: Molecular Diversity of Sea Spray
674 Aerosol Particles: Impact of Ocean Biology on Particle Composition and Hygroscopicity, *Chem.*, 2,
675 655-667, <https://doi.org/10.1016/j.chempr.2017.03.007>, 2017.

676 Collins, D. B., Zhao, D. F., Ruppel, M. J., Laskina, O., Grandquist, J. R., Modini, R. L., Stokes, M. D.,
677 Russell, L. M., Bertram, T. H., Grassian, V. H., Deane, G. B., and Prather, K. A.: Direct aerosol
678 chemical composition measurements to evaluate the physicochemical differences between
679 controlled sea spray aerosol generation schemes, *Atmos Meas Tech*, 7, 3667-3683,
680 <https://doi.org/10.5194/amt-7-3667-2014>, 2014.

681 Cravigan, L. T., Mallet, M. D., Vaattovaara, P., Harvey, M. J., Law, C. S., Modini, R. L., Russell, L. M.,
682 Stelcer, E., Cohen, D. D., Olsen, G., Safi, K., Burrell, T. J., and Ristovski, Z.: Sea spray aerosol
683 organic enrichment, water uptake and surface tension effects, *Atmos Chem Phys*, 20, 7955-7977,
684 <https://doi.org/10.5194/acp-20-7955-2020>, 2020.

685 Czerwiniak, G. A., Russell, S. C., Tobias, H. J., Pitesky, M. E., Fergenson, D. P., Steele, P., Srivastava,
686 A., Horn, J. M., Frank, M., Gard, E. E., and Lebrilla, C. B.: Stable isotope labeling of entire
687 *Bacillus atrophaeus* spores and vegetative cells using bioaerosol mass spectrometry, *Anal Chem*,
688 77, 1081-1087, <https://doi.org/10.1021/ac0488098>, 2005.

689 Dall'Osto, M., Airs, R. L., Beale, R., Cree, C., Fitzsimons, M. F., Beddows, D., Harrison, R. M.,
690 Ceburnis, D., O'Dowd, C., Rinaldi, M., Paglione, M., Nenes, A., Decesari, S., and Simo, R.:
691 Simultaneous Detection of Alkylamines in the Surface Ocean and Atmosphere of the Antarctic
692 Sympagic Environment, *Acs Earth Space Chem*, 3, 854-862,
693 <https://doi.org/10.1021/acsearthspacechem.9b00028>, 2019.

694 Dieckmann, G., Nehrke, G., Uhlig, C., Göttlicher, J., Gerland, S., Granskog, M., and Thomas, D.: Brief
695 Communication: Ikaite (CaCO₃·6H₂O) discovered in Arctic sea ice, *The Cryosphere*, 4, 227-230,
696 <https://doi.org/10.5194/tc-4-227-2010>, 2010.

697 Dieckmann, G., Nehrke, G., Papadimitriou, S., Göttlicher, J., Steininger, R., Kennedy, H., Wolf-
698 Gladrow, D., and Thomas, D.: Calcium carbonate as ikaite crystals in Antarctic sea ice, *Geophys*
699 *Res Lett*, 35 <https://doi.org/10.1029/2008gl033540>, 2008.

700 Facchini, M. C., Rinaldi, M., Decesari, S., Carbone, C., Finessi, E., Mircea, M., Fuzzi, S., Ceburnis, D.,
701 Flanagan, R., Nilsson, E. D., de Leeuw, G., Martino, M., Woeltjen, J., and O'Dowd, C. D.: Primary
702 submicron marine aerosol dominated by insoluble organic colloids and aggregates, *Geophys Res*
703 *Lett*, 35 <https://doi.org/10.1029/2008gl034210>, 2008.

704 Gao, Q., Leck, C., Rauschenberg, C., and Matrai, P. A.: On the chemical dynamics of extracellular

705 polysaccharides in the high Arctic surface microlayer, *Ocean Sci*, 8, 401-418,
706 <https://doi.org/10.5194/os-8-401-2012>, 2012.

707 Gaston, C. J., Furutani, H., Guazzotti, S. A., Coffee, K. R., Bates, T. S., Quinn, P. K., Aluwihare, L. I.,
708 Mitchell, B. G., and Prather, K. A.: Unique ocean-derived particles serve as a proxy for changes in
709 ocean chemistry, *Journal of Geophysical Research: Atmospheres*,
710 116<https://doi.org/10.1029/2010jd015289>, 2011.

711 Gross, D. S., Galli, M. E., Silva, P. J., and Prather, K. A.: Relative sensitivity factors for alkali metal
712 and ammonium cations in single particle aerosol time-of-flight mass spectra, *Anal Chem*, 72, 416-
713 422, <https://doi.org/10.1021/ac990434g>, 2000.

714 Guasco, T. L., Cuadra-Rodriguez, L. A., Pedler, B. E., Ault, A. P., Collins, D. B., Zhao, D. F., Kim, M.
715 J., Ruppel, M. J., Wilson, S. C., Pomeroy, R. S., Grassian, V. H., Azam, F., Bertram, T. H., and
716 Prather, K. A.: Transition Metal Associations with Primary Biological Particles in Sea Spray
717 Aerosol Generated in a Wave Channel, *Environ Sci Technol*, 48, 1324-1333,
718 <https://doi.org/10.1021/es403203d>, 2014.

719 Hara, K., Osada, K., Yabuki, M., and Yamanouchi, T.: Seasonal variation of fractionated sea-salt
720 particles on the Antarctic coast, *Geophys Res Lett*, 39<https://doi.org/10.1029/2012gl052761>, 2012.

721 Keene, W. C., Maring, H., Maben, J. R., Kieber, D. J., Pszenny, A. A. P., Dahl, E. E., Izaguirre, M. A.,
722 Davis, A. J., Long, M. S., Zhou, X. L., Smoydzin, L., and Sander, R.: Chemical and physical
723 characteristics of nascent aerosols produced by bursting bubbles at a model air-sea interface,
724 *Journal of Geophysical Research: Atmospheres*, 112<https://doi.org/10.1029/2007jd008464>, 2007.

725 Kirpes, R. M., Bonanno, D., May, N. W., Fraund, M., Barget, A. J., Moffet, R. C., Ault, A. P., and Pratt,
726 K. A.: Wintertime Arctic Sea Spray Aerosol Composition Controlled by Sea Ice Lead
727 Microbiology, *Acs Central Sci*, 5, 1760-1767, <https://doi.org/10.1021/acscentsci.9b00541>, 2019.

728 Köllner, F., Schneider, J., Willis, M. D., Klimach, T., Helleis, F., Bozem, H., Kunkel, D., Hoor, P.,
729 Burkart, J., Leaitch, W. R., Aliabadi, A. A., Abbatt, J. P. D., Herber, A. B., and Borrmann, S.:
730 Particulate trimethylamine in the summertime Canadian high Arctic lower troposphere, *Atmos
731 Chem Phys*, 17, 13747-13766, <https://doi.org/10.5194/acp-17-13747-2017>, 2017.

732 Köllner, F., Schneider, J., Willis, M. D., Schulz, H., Kunkel, D., Bozem, H., Hoor, P., Klimach, T.,
733 Helleis, F., Burkart, J., Leaitch, W. R., Aliabadi, A. A., Abbatt, J. P. D., Herber, A. B., and
734 Borrmann, S.: Chemical composition and source attribution of sub-micrometre aerosol particles in
735 the summertime Arctic lower troposphere, *Atmos Chem Phys*, 21, 6509-6539,
736 <https://doi.org/10.5194/acp-21-6509-2021>, 2021.

737 Krembs, C., Eicken, H., and Deming, J. W.: Exopolymer alteration of physical properties of sea ice and
738 implications for ice habitability and biogeochemistry in a warmer Arctic, *P Natl Acad Sci USA*,
739 108, 3653-3658, <https://doi.org/10.1073/pnas.1100701108>, 2011.

740 Krembs, C., Eicken, H., Junge, K., and Deming, J. W.: High concentrations of exopolymeric substances
741 in Arctic winter sea ice: implications for the polar ocean carbon cycle and cryoprotection of
742 diatoms, *Deep-Sea Res Pt I*, 49, 2163-2181, [https://doi.org/10.1016/S0967-0637\(02\)00122-X](https://doi.org/10.1016/S0967-0637(02)00122-X),
743 2002.

744 Lawler, M. J., Saltzman, E. S., Karlsson, L., Zieger, P., Salter, M., Baccarini, A., Schmale, J., and Leck,
745 C.: New Insights Into the Composition and Origins of Ultrafine Aerosol in the Summertime High
746 Arctic, *Geophys Res Lett*, 48<https://doi.org/10.1029/2021gl094395>, 2021.

747 Leck, C. and Bigg, E. K.: Source and evolution of the marine aerosol - A new perspective, *Geophys
748 Res Lett*, 32<https://doi.org/10.1029/2005gl023651>, 2005a.

749 Leck, C. and Bigg, E. K.: Biogenic particles in the surface microlayer and overlaying atmosphere in the
750 central Arctic Ocean during summer, *Tellus B*, 57, 305-316, <https://doi.org/10.1111/j.1600-0889.2005.00148.x>, 2005b.

752 Leck, C. and Bigg, E. K.: New Particle Formation of Marine Biological Origin, *Aerosol Sci Tech*, 44,
753 570-577, <https://doi.org/10.1080/02786826.2010.481222>, 2010.

754 Leck, C. and Svensson, E.: Importance of aerosol composition and mixing state for cloud droplet
755 activation over the Arctic pack ice in summer, *Atmos Chem Phys*, 15, 2545-2568,
756 <https://doi.org/10.5194/acp-15-2545-2015>, 2015.

757 Leck, C., Gao, Q., Mashayekhy Rad, F., and Nilsson, U.: Size-resolved atmospheric particulate
758 polysaccharides in the high summer Arctic, *Atmos Chem Phys*, 13, 12573-12588,
759 <https://doi.org/10.5194/acp-13-12573-2013>, 2013.

760 Li, L., Huang, Z., Dong, J., Li, M., Gao, W., Nian, H., Fu, Z., Zhang, G., Bi, X., Cheng, P., and Zhou,
761 Z.: Real time bipolar time-of-flight mass spectrometer for analyzing single aerosol particles, *Int J*
762 *Mass Spectrom*, 303, 118-124, <https://doi.org/10.1016/j.ijms.2011.01.017>, 2011.

763 Liu, Z. M., Lu, X. H., Feng, J. L., Fan, Q. Z., Zhang, Y., and Yang, X.: Influence of Ship Emissions on
764 Urban Air Quality: A Comprehensive Study Using Highly Time-Resolved Online Measurements
765 and Numerical Simulation in Shanghai, *Environ Sci Technol*, 51, 202-211,
766 <https://doi.org/10.1021/acs.est.6b03834>, 2017.

767 Mukherjee, P., Reinfeldt, J. R., and Gao, Y.: Enrichment of calcium in sea spray aerosol in the Arctic
768 summer atmosphere, *Mar Chem*, 227 <https://doi.org/10.1016/j.marchem.2020.103898>, 2020.

769 Murphy, D. M., Anderson, J. R., Quinn, P. K., McInnes, L. M., Brechtel, F. J., Kreidenweis, S. M.,
770 Middlebrook, A. M., Posfai, M., Thomson, D. S., and Buseck, P. R.: Influence of sea-salt on
771 aerosol radiative properties in the Southern Ocean marine boundary layer, *Nature*, 392, 62-65,
772 <https://doi.org/10.1038/32138>, 1998.

773 Norris, S. J., Brooks, I. M., de Leeuw, G., Sirevaag, A., Leck, C., Brooks, B. J., Birch, C. E., and
774 Tjernstrom, M.: Measurements of bubble size spectra within leads in the Arctic summer pack ice,
775 *Ocean Sci*, 7, 129-139, <https://doi.org/10.5194/os-7-129-2011>, 2011.

776 Oppo, C., Bellandi, S., Innocenti, N. D., Stortini, A. M., Loglio, G., Schiavuta, E., and Cini, R.:
777 Surfactant components of marine organic matter as agents for biogeochemical fractionation and
778 pollutant transport via marine aerosols, *Mar Chem*, 63, 235-253, [https://doi.org/10.1016/S0304-4203\(98\)00065-6](https://doi.org/10.1016/S0304-4203(98)00065-6), 1999.

780 Orellana, M. V. and Verdugo, P.: Ultraviolet radiation blocks the organic carbon exchange between the
781 dissolved phase and the gel phase in the ocean, *Limnol Oceanogr*, 48, 1618-1623,
782 <https://doi.org/10.4319/lo.2003.48.4.1618>, 2003.

783 Orellana, M. V., Hansell, D. A., Matrai, P. A., and Leck, C.: Marine Polymer-Gels' Relevance in the
784 Atmosphere as Aerosols and CCN, *Gels*, <https://doi.org/10.3390/gels7040185>, 2021.

785 Orellana, M. V., Matrai, P. A., Leck, C., Rauschenberg, C. D., Lee, A. M., and Coz, E.: Marine
786 microgels as a source of cloud condensation nuclei in the high Arctic, *P Natl Acad Sci USA*, 108,
787 13612-13617, <https://doi.org/10.1073/pnas.1102457108>, 2011.

788 Passig, J., Schade, J., Irsig, R., Li, L., Li, X., Zhou, Z., Adam, T., and Zimmermann, R.: Detection of
789 ship plumes from residual fuel operation in emission control areas using single-particle mass
790 spectrometry, *Atmos Meas Tech*, 14, 4171-4185, <https://doi.org/10.5194/amt-14-4171-2021>, 2021.

791 Prather, K. A., Bertram, T. H., Grassian, V. H., Deane, G. B., Stokes, M. D., DeMott, P. J., Aluwihare, L.
792 I., Palenik, B. P., Azam, F., Seinfeld, J. H., Moffet, R. C., Molina, M. J., Cappa, C. D., Geiger, F.

793 M., Roberts, G. C., Russell, L. M., Ault, A. P., Baltrusaitis, J., Collins, D. B., Corrigan, C. E.,
794 Cuadra-Rodriguez, L. A., Ebben, C. J., Forestieri, S. D., Guasco, T. L., Hersey, S. P., Kim, M. J.,
795 Lambert, W. F., Modini, R. L., Mui, W., Pedler, B. E., Ruppel, M. J., Ryder, O. S., Schoepp, N. G.,
796 Sullivan, R. C., and Zhao, D. F.: Bringing the ocean into the laboratory to probe the chemical
797 complexity of sea spray aerosol, *P Natl Acad Sci USA*, 110, 7550-7555,
798 <https://doi.org/10.1073/pnas.1300262110>, 2013.

799 Pratt, K. A. and Prather, K. A.: Mass spectrometry of atmospheric aerosolsuRecent developments and
800 applications. Part II: On-line mass spectrometry techniques, *Mass Spectrom Rev*, 31, 17-48,
801 <https://doi.org/10.1002/mas.20330>, 2012.

802 Pratt, K. A., DeMott, P. J., French, J. R., Wang, Z., Westphal, D. L., Heymsfield, A. J., Twohy, C. H.,
803 Prenni, A. J., and Prather, K. A.: In situ detection of biological particles in cloud ice-crystals, *Nat*
804 *Geosci*, 2, 397-400, <https://doi.org/10.1038/Ngeo521>, 2009.

805 Qin, X. Y., Bhawe, P. V., and Prather, K. A.: Comparison of two methods for obtaining quantitative
806 mass concentrations from aerosol time-of-flight mass spectrometry measurements, *Anal Chem*, 78,
807 6169-6178, <https://doi.org/10.1021/ac060395q>, 2006.

808 Quinn, P. K., Collins, D. B., Grassian, V. H., Prather, K. A., and Bates, T. S.: Chemistry and Related
809 Properties of Freshly Emitted Sea Spray Aerosol, *Chem Rev*, 115, 4383-4399,
810 <https://doi.org/10.1021/cr500713g>, 2015.

811 Rankin, A. M., Wolff, E. W., and Martin, S.: Frost flowers: Implications for tropospheric chemistry and
812 ice core interpretation, *Journal of Geophysical Research: Atmospheres*, 107, AAC 4-1-AAC 4-15,
813 <https://doi.org/10.1029/2002jd002492>, 2002.

814 Russell, L. M., Hawkins, L. N., Frossard, A. A., Quinn, P. K., and Bates, T. S.: Carbohydrate-like
815 composition of submicron atmospheric particles and their production from ocean bubble bursting,
816 *P Natl Acad Sci USA*, 107, 6652-6657, <https://doi.org/10.1073/pnas.0908905107>, 2010.

817 Salter, M. E., Hamacher-Barth, E., Leck, C., Werner, J., Johnson, C. M., Riipinen, I., Nilsson, E. D.,
818 and Zieger, P.: Calcium enrichment in sea spray aerosol particles, *Geophys Res Lett*, 43, 8277-
819 8285, <https://doi.org/10.1002/2016gl070275>, 2016.

820 Schill, S. R., Collins, D. B., Lee, C., Morris, H. S., Novak, G. A., Prather, K. A., Quinn, P. K., Sultana,
821 C. M., Tivanski, A. V., Zimmermann, K., Cappa, C. D., and Bertram, T. H.: The Impact of Aerosol
822 Particle Mixing State on the Hygroscopicity of Sea Spray Aerosol, *Acs Central Sci*, 1, 132-141,
823 <https://doi.org/10.1021/acscentsci.5b00174>, 2015.

824 Sierau, B., Chang, R. Y. W., Leck, C., Paatero, J., and Lohmann, U.: Single-particle characterization of
825 the high-Arctic summertime aerosol, *Atmos Chem Phys*, 14, 7409-7430,
826 <https://doi.org/10.5194/acp-14-7409-2014>, 2014.

827 Sievering, H.: Aerosol non-sea-salt sulfate in the remote marine boundary layer under clear-sky and
828 normal cloudiness conditions: Ocean-derived biogenic alkalinity enhances sea-salt sulfate
829 production by ozone oxidation, *Journal of Geophysical Research: Atmospheres*,
830 109<https://doi.org/10.1029/2003jd004315>, 2004.

831 Song, C., Becagli, S., Beddows, D. C. S., Brean, J., Browse, J., Dai, Q., Dall'Osto, M., Ferracci, V.,
832 Harrison, R. M., Harris, N., Li, W., Jones, A. E., Kirchgäßner, A., Kramawijaya, A. G., Kurganskiy,
833 A., Lupi, A., Mazzola, M., Severi, M., Traversi, R., and Shi, Z.: Understanding Sources and
834 Drivers of Size-Resolved Aerosol in the High Arctic Islands of Svalbard Using a Receptor Model
835 Coupled with Machine Learning, *Environ Sci Technol*, 56, 11189-11198,
836 <https://doi.org/10.1021/acs.est.1c07796>, 2022.

837 Song, X. and Hopke, P. K.: Classification of single particles analyzed by ATOFMS using an artificial
838 neural network, *ART-2A, Anal Chem*, 71, 860-865, <https://doi.org/10.1021/ac9809682>, 1999.

839 Srivastava, A., Pitesky, M. E., Steele, P. T., Tobias, H. J., Fergenson, D. P., Horn, J. M., Russell, S. C.,
840 Czerwieniec, G. A., Lebrilla, C. S., Gard, E. E., and Frank, M.: Comprehensive assignment of
841 mass spectral signatures from individual *Bacillus atrophaeus* spores in matrix-free laser
842 desorption/ionization bioaerosol mass spectrometry, *Anal Chem*, 77, 3315-3323,
843 <https://doi.org/10.1021/ac048298p>, 2005.

844 Su, B., Wang, T., Zhang, G., Liang, Y., Lv, C., Hu, Y., Li, L., Zhou, Z., Wang, X., and Bi, X.: A review
845 of atmospheric aging of sea spray aerosols: Potential factors affecting chloride depletion, *Atmos*
846 *Environ*, 290 <https://doi.org/10.1016/j.atmosenv.2022.119365>, 2022.

847 Su, B. J., Zhuo, Z. M., Fu, Y. Z., Sun, W., Chen, Y., Du, X. B., Yang, Y. X., Wu, S., Xie, Q. H., Huang,
848 F. G., Chen, D. H., Li, L., Zhang, G. H., Bi, X. H., and Zhou, Z.: Individual particle investigation
849 on the chloride depletion of inland transported sea spray aerosols during East Asian summer
850 monsoon, *Sci Total Environ*, 765 <https://doi.org/10.1016/j.scitotenv.2020.144290>, 2021.

851 Sullivan, R. C., Moore, M. J. K., Petters, M. D., Kreidenweis, S. M., Roberts, G. C., and Prather, K. A.:
852 Timescale for hygroscopic conversion of calcite mineral particles through heterogeneous reaction
853 with nitric acid, *Phys Chem Chem Phys*, 11, 7826-7837, <https://doi.org/10.1039/b904217b>, 2009.

854 Tobo, Y., Adachi, K., DeMott, P. J., Hill, T. C. J., Hamilton, D. S., Mahowald, N. M., Nagatsuka, N.,
855 Ohata, S., Uetake, J., Kondo, Y., and Koike, M.: Glacially sourced dust as a potentially significant
856 source of ice nucleating particles, *Nat Geosci*, 12, 253-258, [https://doi.org/10.1038/s41561-019-](https://doi.org/10.1038/s41561-019-0314-x)
857 [0314-x](https://doi.org/10.1038/s41561-019-0314-x), 2019.

858 Vancoppenolle, M., Meiners, K. M., Michel, C., Bopp, L., Brabant, F., Carnat, G., Delille, B., Lannuzel,
859 D., Madec, G., Moreau, S., Tison, J.-L., and van der Merwe, P.: Role of sea ice in global
860 biogeochemical cycles: emerging views and challenges, *Quaternary Science Reviews*, 79, 207-230,
861 <https://doi.org/10.1016/j.quascirev.2013.04.011>, 2013.

862 Verdugo, P.: Marine microgels, *Annual Review of Marine Science*, 4, 375-400,
863 <https://doi.org/10.1146/annurev-marine-120709-142759>, 2012.

864 Verdugo, P., Alldredge, A. L., Azam, F., Kirchman, D. L., Passow, U., and Santschi, P. H.: The oceanic
865 gel phase: a bridge in the DOM-POM continuum, *Mar Chem*, 92, 67-85,
866 <https://doi.org/10.1016/j.marchem.2004.06.017>, 2004.

867 Wang, Y. Q.: MeteoInfo: GIS software for meteorological data visualization and analysis, *Meteorol.*
868 *Appl.*, 21, 360-368, <https://doi.org/10.1002/met.1345>, 2014.

869 Wang, Y. Q., Zhang, X. Y., and Draxler, R. R.: TrajStat: GIS-based software that uses various trajectory
870 statistical analysis methods to identify potential sources from long-term air pollution measurement
871 data, *Environ Modell Softw*, 24, 938-939, <https://doi.org/10.1016/j.envsoft.2009.01.004>, 2009.

872 Willis, M. D., Leaitch, W. R., and Abbatt, J. P. D.: Processes Controlling the Composition and
873 Abundance of Arctic Aerosol, *Rev Geophys*, 56, 621-671, <https://doi.org/10.1029/2018rg000602>,
874 2018.

875 Wilson, T. W., Ladino, L. A., Alpert, P. A., Breckels, M. N., Brooks, I. M., Browse, J., Burrows, S. M.,
876 Carslaw, K. S., Huffman, J. A., Judd, C., Kilhau, W. P., Mason, R. H., McFiggans, G., Miller, L.
877 A., Najera, J. J., Polishchuk, E., Rae, S., Schiller, C. L., Si, M., Temprado, J. V., Whale, T. F.,
878 Wong, J. P., Wurl, O., Yakobi-Hancock, J. D., Abbatt, J. P., Aller, J. Y., Bertram, A. K., Knopf, D.
879 A., and Murray, B. J.: A marine biogenic source of atmospheric ice-nucleating particles, *Nature*,
880 525, 234-238, <https://doi.org/10.1038/nature14986>, 2015.

881 Yan, J., Jung, J., Lin, Q., Zhang, M., Xu, S., and Zhao, S.: Effect of sea ice retreat on marine aerosol
882 emissions in the Southern Ocean, Antarctica, *Sci Total Environ*, 745, 140773,
883 <https://doi.org/10.1016/j.scitotenv.2020.140773>, 2020a.

884 Yan, J., Jung, J., Zhang, M., Xu, S., Lin, Q., Zhao, S., and Chen, L.: Significant Underestimation of
885 Gaseous Methanesulfonic Acid (MSA) over Southern Ocean, *Environ Sci Technol*, 53, 13064-
886 13070, <https://doi.org/10.1021/acs.est.9b05362>, 2019.

887 Yan, J., Jung, J., Zhang, M., Bianchi, F., Tham, Y., Xu, S., Lin, Q., Zhao, S., Li, L., and Chen, L.:
888 Uptake selectivity of methanesulfonic acid (MSA) on fine particles over polynya regions of the
889 Ross Sea, Antarctica, *Atmos Chem Phys*, 20, 3259-3271, [https://doi.org/10.5194/acp-20-3259-](https://doi.org/10.5194/acp-20-3259-2020)
890 [2020](https://doi.org/10.5194/acp-20-3259-2020), 2020b.

891 Yang, X., Pyle, J. A., and Cox, R. A.: Sea salt aerosol production and bromine release: Role of snow on
892 sea ice, *Geophys Res Lett*, 35<https://doi.org/10.1029/2008gl034536>, 2008.

893 Young, L.-H., Li, C.-H., Lin, M.-Y., Hwang, B.-F., Hsu, H.-T., Chen, Y.-C., Jung, C.-R., Chen, K.-C.,
894 Cheng, D.-H., Wang, V.-S., Chiang, H.-C., and Tsai, P.-J.: Field performance of a semi-continuous
895 monitor for ambient PM_{2.5} water-soluble inorganic ions and gases at a suburban site, *Atmos*
896 *Environ*, 144, 376-388, <https://doi.org/10.1016/j.atmosenv.2016.08.062>, 2016.

897 Zawadowicz, M. A., Froyd, K. D., Murphy, D. M., and Cziczo, D. J.: Improved identification of
898 primary biological aerosol particles using single-particle mass spectrometry, *Atmos Chem Phys*, 17,
899 7193-7212, <https://doi.org/10.5194/acp-17-7193-2017>, 2017.

900 Zhang, T., Fiamingo, M., and Allen, H. C.: Trace Metal Enrichment Driven by Phosphate Functional
901 Group Binding Selectivity, *Journal of Geophysical Research: Oceans*, 123, 5286-5297,
902 <https://doi.org/10.1029/2018jc013926>, 2018.

903